Hall Thruster Plume Effects on Spacecraft Charging from 0.067 AU to 1 AU

T. L. Shinde[1,2,3], Iver H. Cairns[2,3], Jason. M. Held[2,3], and Gregoire Deprez[4]

https://orcid.org/0000-0003-4576-6627, https://orcid.org/0000-0001-6978-9765, https://orcid.org/0000-0002-6803-0287, https://orcid.org/0009-0000-7586-0249

[1] School of Physics, University of Sydney, NSW 2006, Australia,[2] The Australian Research Council Training Centre for CubeSats, UAVs, and Their Applications (CUAVA),[3] Saber Astronautics, Sydney, NSW 2008, Australia, [4] European Space Agency, 2201 AZ, Noordwijk, The Netherlands

Corresponding author: T. L. Shinde (tej.shinde2425@gmail.com)

Key Points:

- Hall thrusters achieve a stable negative spacecraft potential across diverse heliocentric conditions.
- Thruster reduces ion-wake potentials, minimizing spacecraft charging in near-sun environments, showcasing its vital role.
- SPIS software is used to analyse charging effects on spacecraft with and without a Hall thruster across various heliocentric distances.

Abstract

The backflow plume from an electric thruster can lead to the accumulation of electrostatic charge on the spacecraft, leading to a negative charge. Interactions between the plume and solar wind can further influence the charge distribution, resulting in variations in spacecraft potential and interference with sensitive instruments. A 3D Particle-In-Cell (PIC) simulation tool within the Spacecraft Plasma Interaction Software (SPIS) is used to compute spacecraft charging effects from 0.067 to 1 Astronomical unit (AU). The study examines the dynamic behaviour of ambient electrons and ions, thruster electrons, and CEX-ions, as well as photoemission and secondary electrons, and solar photon flux impact on the spacecraft potential. The main finding is the demonstration that the high dominance of CEX-ions and thruster electrons helps to achieve a low and stable negative potential ranging from -2 to -6 V from 0.067 AU to 1 AU when the thruster is on, as opposed to the varying range of -5 to +9 V with the thruster off. Other findings are that the elimination of photoelectrons or secondary electrons has a comparatively greater impact on spacecraft potential when the thruster is off, as opposed to when the thruster is on. Both CEX-ions and thruster electrons significantly contribute to the mitigation and regulation of spacecraft potential towards a less negative potential in situations where photoemission or secondary electrons are absent or relatively unimportant.

Plain Language Summary

As a spacecraft travels through space, it encounters a mix of charged particles from its surroundings. These particles strike the spacecraft's surface, causing it to accumulate an electrostatic charge. This charge can be either positive or negative, depending on the density and temperature of incoming electrons and ions and the solar photon flux. A current balance is achieved when the incoming and outgoing currents of charged particles equalize. Additionally, external sources such as electric thrusters, which are crucial for propulsion, emit various charged particles. The combined effects of the space environment and externally charged particles create a complex interaction that results in spacecraft charging. In certain instances, spacecraft can accumulate an excessive negative or positive charge, leading to significant anomalies and mission failures. This paper demonstrates that the operation of a Hall thruster can strongly limit this charging and keep the spacecraft at a low negative, stable, potential from close to the Sun to near Earth. The research will aid in spacecraft design and the positioning of instruments to prevent operational issues arising from spacecraft charging.

1 Introduction

In recent years, there has been a growing interest in electric propulsion systems for commercial, scientific, and interplanetary missions, mainly due to their high specific impulse, thruster controllability, and proven reliability (e.g., in Geobel & Katz, 2008; Kuninaka et al., 2011; Garner & Liu et al., 2013). Electric thrusters offer higher delta-V compared to chemical propulsion which allows additional payload capacity (Geobel & Katz, 2008). However, it's important to note that electric propulsion systems have some drawbacks. One significant drawback is the significantly longer time-to-destination compared to chemical propulsion systems. The prolonged journey increases the risk of major changes in the spacecraft charging while passing through the solar wind environment (e.g., in Geobel & Katz, 2008; Liu et al., 2013). The solar wind's particles can cause variations in the spacecraft's electrostatic potential, severely disturbing low-energy particle and electric field measurements shown by Guillemant (2013). Additionally, when an electric thruster operates in different plasma environments, spacecraft surface charging variations are expected (e.g., in Wang (1997) and Feng et al. (2019). The effects caused by electric thruster operations have long raised both scientific and operational concerns. The plume's backflow can contaminate and interact with spacecraft payload systems, potentially leading to unfavourable consequences for the mission lifetime (e.g., in Wang 1997; Tajmar 2002; Reissner et al., 2011; Feng et al., 2019, Filleul et al., 2021).

Backflow plumes from an electric thruster consist of low-velocity charge-exchange ions (CEX-ions) that result from collisions between fast-beam ions and propellant neutrals within the main ion beam and the

thruster electrons emitted from the cathode as discussed in Geobel & Katz (2008). These low-energy ions and electrons flow back toward the spacecraft, giving rise to two primary effects. Firstly, the deposition of effluent causes contamination on optical sensors, solar arrays, thermal control systems, and other communication devices. Secondly, the presence of CEX-ions and associated electrons modify the properties of the solar wind surrounding the spacecraft, leading to an additional current that can influence the spacecraft potential and plasma instrument observations as discussed in Wang (1997). Consequently, studying thruster-induced plasma and solar wind effects on spacecraft charging in different environments is crucial to avoid operational and measurement anomalies and failures. However, performing such complex interaction measurements in a vacuum chamber presents challenges due to the physical scale of the system and the inability to fully replicate the solar wind environment, making it time-consuming, often inaccurate and expensive. Therefore, numerical simulations play a vital role in predicting thruster-spacecraft interactions and provide a more comprehensive way to gain valuable insights into charging characteristics compared to ground testing.

Referring to solar wind effects on spacecraft charging at various heliocentric distances, Guillemant (2013) investigated variations in spacecraft potential, electrostatic sheath, and potential barrier with the distance to the Sun using the Spacecraft Plasma Interaction Software (SPIS). The simulation result revealed that the spacecraft charged positively by a few volts from 1 AU to around 0.3 AU. However, within 0.3 AU, the potential barrier generated by photoelectrons and secondary electrons caused the potential to become negative. These low-energy electrons tended to surround the spacecraft, generating a potential barrier that significantly affected the plasma potential and led to the high recollection of low-energy electrons. Consequently, these low-energy electrons could interfere with plasma sensors and particle detectors, biasing the particle distribution functions measured by the instruments as shown in Guillemant (2013).

Numerical simulations conducted by several researchers explore the interaction between the spacecraft surface and the thruster plume. A consistent finding across simulations is the significant impact of the backflow plume of charge-exchange (CEX) ions since their density is much higher compared to the ambient density, as documented in various studies (Wang 1997; Tajmar et al., 2002; Reissner et al., 2011; Feng et al., 2019; Filleul et al., 2021). Acting as a neutralizer, CEX ions and thruster electrons play a crucial role in mitigating the negative potential of the spacecraft. Feng et al. (2019), derived important insights from real flight data collected from the SMART-1 spacecraft. Notably, it was observed that two species of CEX-ions had energies of 35 and 65eV. The first one is dominant and due to single-charged ions, while the second group is due to double-charged ions. The doubly charged CEX-ions can be neglected since their density is much smaller than singly charged ions. In a separate flight, Torkar et al. (2001), noted that the Cluster spacecraft acquired a high positive potential, due to substantial currents from photoelectrons. The strong electrostatic sheath enveloping the spacecraft introduced disruptions in particle and electric field measurements. To mitigate this challenge, the Cluster spacecraft integrated an indium ion emitter, capable of producing ions within the 5 to 9 keV energy range, at currents ranging in the tens of microamperes. The Active Spacecraft Potential Controller (ASPOC), an instrument aboard the Cluster spacecraft, showcased significant reductions in spacecraft potential, leading to enhancements in particle measurements, see Torkar et al. (2001). Similar favourable outcomes were also observed in the case of the Double Star TC-1 spacecraft by Torkar et al. (2005). The phenomenon demonstrates the benefits of a positive ion beam's presence in lowering and stabilizing the potential, reducing potential variation, and enhancing particle measurements.

Nevertheless, the understanding of these complex interactions and their implications for spacecraft potential remains elusive, particularly considering variations in solar wind conditions, the presence or absence of photoelectrons, and secondary electrons. Consequently, the aim of our research investigate ion-induced charging effects on spacecraft potential across various heliocentric distances using the Spacecraft Plasma Interaction Software (SPIS). The investigation will be based on factors involving ambient electrons and ions, secondary electrons and photoelectrons, CEX-ions and thruster electrons, and solar photon flux.

In our first conference paper, the impact of the SPT-100 Hall thruster on spacecraft potential at heliocentric distances of 1 AU and 0.093 AU was examined by Shinde et al. (2022). The results revealed that both CEX-ions and thruster electrons dominate the satellite's plasma environment at both distances, resulting in negative spacecraft potentials due to the higher thruster electron impact rate. Moreover, at 0.093 AU, the effects of photoelectrons and secondary electrons become slightly more significant than at 1AU, leading to more positive spacecraft potentials. Another study by Shinde et al. (2023) showed the ion-induced charging effects from 0.044 AU to 1 AU by comparing spacecraft potential variations and current assessments for various sources with the thruster on and off. The study demonstrated that electric thrusters can effectively maintain a low and negative potential over a wide range of heliocentric distances. Notably, when the thruster is active, a substantial reduction in the spatial size of the sheath and the potential barrier was observed. However, it's important to note that the study by Shinde et al. (2023) did not account for the inverse distance squared fall-off of the solar photon flux.

The present paper aims to investigate the effects of various factors on spacecraft charging in different solar wind conditions when the SPT-100 Hall thruster is switched on and off. These factors include ambient electrons and ions, thruster electrons and CEX-ions, photoemission and secondary electrons, and the solar photon flux at different heliocentric distances. The spatial profiles of the ram, wake, and electrostatic sheath structure for all heliocentric distances will also be examined. To achieve this, the SPIS software will be used for simulation setup and physical parameter modelling (Section 2). The paper will then show the result in section 3. Section 3.1 shows the analysis of the spacecraft potential variation and derives a best-fit equation for conditions with and without the thruster across the range from 0.067 AU to 1 AU. Additionally, the collected and emitted currents on the satellite's surface will be studied under different thruster conditions (section 3.2). The detailed potential profiles of the ram, wake, and sheath surrounding the spacecraft will be presented in Section 3.3. Section 3.4 will focus on the role of secondary electrons at 0.067 AU and 1 AU, both with and without the thruster. The importance of photoelectrons in influencing spacecraft potential will be discussed in Section 3.5 for these distances, with and without the thruster. Finally, in Section 3.6, the combined effect of neglecting secondary electrons and photoelectrons on spacecraft potential will be examined at 0.067 AU and 1 AU, with and without the thruster. By addressing these aspects comprehensively, the paper aims to provide a thorough understanding of spacecraft charging in different solar wind conditions and the influence of the SPT-100 Hall thruster on spacecraft potential.

2 Simulation setup

Spacecraft Plasma Interaction Software (SPIS) version 6.1.0 is an open-source simulation tool which solves the electrostatic potential and motion of charged and neutral particles in 3D, using an unstructured mesh, around a spacecraft with complex and realistic geometries to compute spacecraft-plasma interactions, variations in spacecarft potential, and detailed sheath structures around a spacecraft. SPIS simulations are based on the Particle In Cell method (PIC) but it offers the possibility to switch between different versions of the PIC method like full-PIC (where all charged species are modelled as particles) or hybrid-PIC, where electrons are simulated as a fluid (e.g., in Wartelski et al., 2011 & Sarrailh et al., 2015). The simulation tool is widely employed for spacecraft charging simulations in different environments such as in LEO, GEO, and electric thruster operations, see (e.g., in Reissner 2011; Wartelski et al., 2011, 2013; Thiebault et al., 2015; & Filleul et al., 2021). The spacecraft charging is determined through an equivalent electric circuit, accounting for its interaction with the surrounding plasma, calculating the currents between the plasma and spacecraft using a circuit solver. Within SPIS, the spacecraft potential is obtained by solving a linear or non-linear Poisson equation for densities typical of most electric thrusters; the quasi-neutrality assumption (which also assumes the Boltzmann relation) yields the same outcome as solving the Poisson equation, offering a faster and more stable solution shown in (e.g., Bigioni et al., 2003 & Wartelski et al., 2011). Therefore, it is possible to implement in SPIS the quasi-neutrality equations with constant or variable electron temperature. Nevertheless, the user can switch between the Poisson solver and the quasi-neutrality approach from the SPIS Graphical User Interface (GUI). If the quasi-neutrality approach with a

constant electron temperature is selected, the plasma potential is calculated from Equation 1 given in Wartelski et al. (2011):

$$\Phi_p = \frac{k_b T_e}{e} \; . ln \frac{n_i}{n_{ref}} + \Phi_{ref} \; , \qquad (1)$$

where Φ_p is plasma potential [in V], k_b is Boltzmann's constant, T_e is the electron temperature [in eV], e is elementary charge, n_i is ion density, and n_{ref} and Φ_{ref} are respectively the plasma density and the plasma potential at a certain point. This Boltzmann relation only holds for isothermal, unmagnetized, and collisionless electrons.

For full PIC modelling, the 3D mesh resolution in the simulation domain must be finer than that of the local Debye length to resolve the sheath and electron dynamics, see Fileul et al.,, (2021). Given the extremely small Debye length downstream of the thruster it is computationally demanding to meet the mesh resolution of the simulations. Hence an alternative method is chosen to treat the neutralizer electrons as an isothermal fluid population (all electrons are assumed to have the same temperature throughout the simulation). The electron density over the simulation mesh is then determined by the local plasma potential according to Boltzmann's relation, thus simplifying the simulation, as explained in Filleul et al., (2021). Further in order to simplify and accurately model the thruster plume and spacecarft interactions, quasineutrality was assumed (where ne=ni), for a nonisothermal fluid electron population using a polytropic law, as shown by Wartelski et al. (2011) & Filleul et al. (2021). The polytropic law describes how the pressure and density of electrons vary despite the code limitation.

$$T_e \, n_e^{\,1-\gamma} = C, \qquad (2)$$

where γ is the polytropic constant (with γ=1 corresponding to the isothermal case and γ=5/3 for an adiabatic plasma) and C is a temperature constant. However, this led to a major drawback as explained in. Filleul et al., (2021), where the forced quasineutrality showed an inability to accurately describe the sheath near the spacecraft. Hence the polytropic constant was varied between the isothermal case (γ=1) and the adiabatic one (γ=5/3) to obtain the influence of spacecraft-plume interaction. Finally, the only available solution to address the computational limitation was to combine Equation (2) and the Vlasov equation with the quaineutrality hypothesis to obtain the electric potential as the following Equation 3 given in Wartelski et al. (2011) & Filleul (2021):

$$\Phi_p = \frac{k_b \, \gamma \, T_{e,ref}}{e \, (\gamma - 1)} \left[\left(\frac{n_i}{n_{ref}} \right)^{\gamma - 1} \right] + \Phi . \qquad (3)$$

The spacecarft model in our paper will calculate the spacecarft potential near the spacecarft in the presence of thruster CEX-ions and thruster electrons using Equation 3.

The Hall thruster model in SPIS utilizes a Monte-Carlo method (MCC) to simulate collisions between CEX-ions and various other species (neutral Xe, Xe+, and Xe++) within the computational regions. For thrusters using Xenon, only the following two charge-exchange collisions are simulated:

$$Xe^{+}_{fast} + Xe_{slow} \rightarrow Xe_{fast} + Xe^{+}_{slow} \qquad (4)$$

$$Xe^{++}_{fast} + Xe_{slow} \rightarrow Xe_{fast} + Xe^{++}_{slow} \qquad (5)$$

Xe_{fast} particles do not contribute significantly to charging and Xe_{slow} is assumed not to be modified by collisions, since ion-ion and ion-neutral elastic collisions are ignored as justified in Wartelski et al. (2011).

Earlier work of Wartelski et al. (2011, 2013) provides justifications for the accuracy of plume models for various electric thrusters in SPIS, demonstrating a strong correlation between experimental, in-flight, data and simulated outcomes. More detailed information about SPIS and its modelling capabilities can be found in the work of Sarrailh et al. (2015).

The setup for the simulation involves specifying the spacecraft's geometry, computational mesh, material properties, internal circuitry, and the simulated environment. In this paper, we adopt the same spacecraft model employed in our prior research (Shinde et al., 2022, 2023) representing it as a cylinder with a 1m radius and a 2 m long, coated with indium tin oxide (ITO) material. The dimensions of the simulation domain vary based on the Debye length, and accordingly, we apply mesh refinement. The domain dimension must be smaller than three times the thermal electron's Debye length (3 x Debye length). Meanwhile, the mesh resolution within the domain is always less than one-third of the Debye length, resulting in 50,000 to 100,000 mesh tetrahedrons. The spacecraft mesh size is based on the thermal and photoelectron electron Debye lengths (one-third of the local plasma Debye length). The model for the satellite is created using Gmsh software, version 4.10.5 (which is free software to generate a mesh geometry, and to perform post-processing, available online at https://gmsh.info/), as shown in Figure 1 and Table 1. The physical parameters for simulating various heliocentric distances are adopted from Guillemant (2013) as shown in Table 2. The simulation considers varying plasma properties, such as density, temperature, and bulk velocity, varying photon flux, and timesteps for ions, thermal electrons, secondary electrons, and photoelectrons. Additionally, the solar photon flux is taken into account. For simplification, the satellite is assumed to be stationary relative to the Sun. Therefore, only the solar wind ion drift velocity, directed along the x-axis, is simulated. The corresponding electron drift is neglected since it is small compared with the electron thermal speed, which is not true for the ions.

During the simulations, the thruster is assumed to be electrically isolated from the spacecraft chassis, while the spacecraft surface floats with the plasma. The anode and cathode of the thruster are isolated from the spacecraft using a resistor. To manage excessive charging, a 500-kilo Ohm resistor is introduced between the thruster and the spacecraft, providing a return path for leakage currents. The resistor ensures a high degree of isolation between the thruster and the spacecraft surface, thereby limiting potential charging issues (Liu et al. 2013). It is crucial to note that the ground of the spacecraft is distinct from the ground of the electric thrusters. This configuration is adopted primarily to reduce spacecraft contamination caused by the thruster plumes as discussed in Liu et al. (2013). During the simulations, the magnetic field and backscattered electrons are not considered. Figure 1 shows the centre of the cylinder representing the spacecraft located at the origin of the Cartesian coordinate system (0, 0, 0). The orientation of the plane is as follows: the x-axis points along the thruster axis (i.e., the length of the cylinder), the y-axis points vertically upward along the plane of the paper, and the z-axis points outward from the plane.

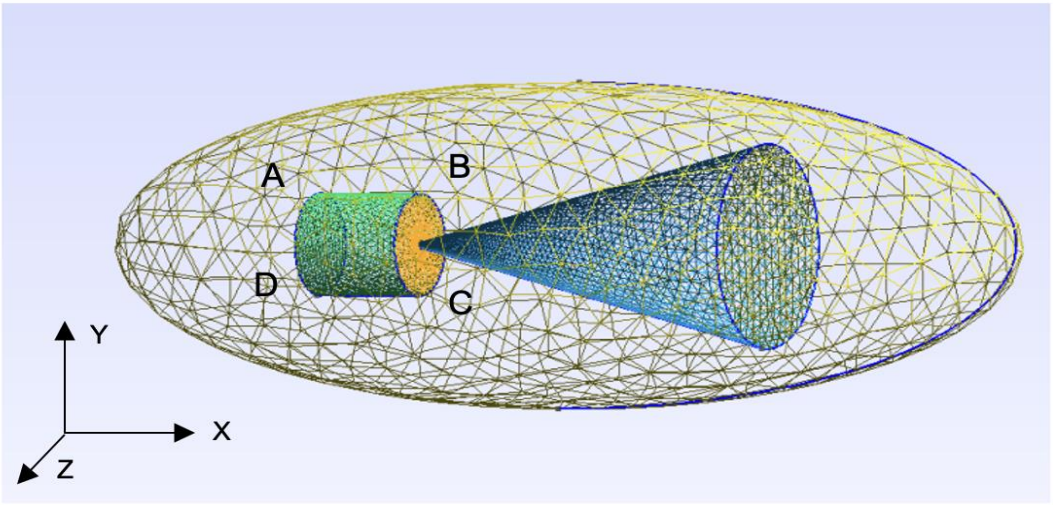

Figure 1. GMSH spacecraft model with a meshing grid (green/yellow), the void boundary is the simulation boundary, and the blue conical shape represents the ion plume.

Table 1

Gmsh Geometry Dimensions and Thruster Specifications.

Parameters	**Value**
Geometry	1m radius, 2m long, cylinder
Surface Material	Indium Tin Oxide
Photoelectron temperature	3eV
Thruster Electron Temperature	0.5-0.8eV
Ambient Ion type	H+
Ion modelling	PIC
Electron modelling	PIC
Magnetic Field	Not considered
Thruster Specification	
Ion Thruster	SPT-100 Hall
Thrust	0.035 N
Specific Impulse	1840s
Cathode Temperature	5 eV
Mass Flow rate (Xe)	1.91×10^{-6} Kg/s
Current	1.43 A
Power	723 W

Table 2

Physical Parameters Used in SPIS To Simulate Various Environments Charging Effects from Guillemant, (2013)

Distance (AU)	**1**	**0.42**	**0.72**	**0.25**	**0.162**	**0.11**	**0.093**	**0.067**	**0.044**
Solar Flux	1	1.93	4.73	16.0	38.10	82.64	115.62	222.7	516.53
$N_e=N_i$ (m^{-3})	6.93e6	1.35e7	3.67e7	1.19e8	3.10e8	8.03e8	1.14e9	1.94e9	7.0e9
T_e (eV)	8.14	10.41	14.52	22.95	31.77	41.50	48.33	59.25	84.47

T_i (eV)	8.00	11.21	17.00	30.76	39.90	49.00	55.82	67.00	87.25
V ram (km/s)	430.00	429.00	400.00	401.40	366.00	355.00	350.00	335.00	300.00
Debye length (m)	8.06	6.52	4.67	3.27	2.38	1.69	1.53	1.30	0.82
Debye length of photoelectrons (m)	0.98	0.71	0.45	0.25	0.16	0.11	0.09	0.07	0.04
Secondaries T_e (eV)	0.28	0.35	0.45	0.7	0.95	1.2	1.32	1.55	1.92

3. Results

3.1. Variations of the Potential from 0.067 AU to 1 AU

Figure 2 shows the variation in spacecraft potential for a wide range of heliocentric distances with and without the thruster. The dotted curve indicates the spacecraft potential without the solar photon flux while the solid curves are with the solar photon flux. Consider a distance greater than 0.25 AU, without the thruster, where the charging effects are less critical compared with a near- Sun environment. The region is dominated by photoelectrons (without the thruster) due to their much higher density of 10^8 m^{-3} compared to other number densities (ambient ions 10^7 $m^{-3.}$, thermal electron 10^7 m^{-3}, secondaries 10^7 m^{-3}) which all vary with the inverse squared distance from the Sun, see Shinde et al. (2022). The decreasing mean energy of thermal electrons reduces the secondary emission rate. Moreover, the ambient ions become a source of secondary electrons due to proton impact (SEEP) on the spacecraft surface and so increase the secondary electron density. As shown in Figure 2, outside 0.25 AU the spacecraft potential (without the thruster) is positive and decreases monotonically with increasing distance. The positive charging of the spacecraft can be explained by the emission of photoelectrons in the thick sheath approximation, which holds validity in this instance Guillemant (2013). This is also referred to as the Orbital Motion Limited model, where spacecraft charging is affected by the spacecraft's motion through the surrounding plasma as explained in Guillemant (2013). When the Debye length of photoelectrons is greater than the spacecraft's size, the potential barrier (shown in section 3.3) does not impede the escape of photoelectrons and secondary particles, thereby resulting in the spacecraft's positive charging. The recollection of secondary electrons in this region is simply because of the positive potential of the spacecraft.

Below 0.25 AU, close to the Sun, the spacecraft charging effects become more critical due to the hot and dense ambient environment, despite higher photoemission and secondary emission rates from the surfaces exposed to the plasma. As shown in Figure 2 without the thruster, the satellite potential decreases to -28.6 V at 0.044 AU. The negative charging can be explained by the fact that the high thermal electron density of 10^9 m^{-3} and temperature of about 100 eV dominate and charge the spacecraft negatively despite the high photoemission - see e.g., Guillemant (2013) & Ergun et al. (2010). This result might appear contradictory when considering photoemission, but it can be explained by the fact that the temperature of thermal electrons is much higher compared to that of photoelectrons and secondary electrons. As a result, the local potential barrier (detailed explanation in section 3.3) comes closer to the surface, restricting the escape of photoelectrons and secondary electrons, and leading to a high level of re-collection. Guillemant's (2013) study shows that the recollection of photoelectrons and secondary electrons is extremely efficient in achieving a current balance with a negative spacecraft potential. This phenomenon corresponds to a thin sheath, also known as the space-charge limited model, which holds true when the Debye length of photoelectrons is smaller than the spacecraft size (for a detailed explanation see Guillemant (2013). In such

cases, spacecraft charging is primarily influenced by the space charge, which dominates plasma behaviour. In the previously reported paper by Shinde et al. (2023), similar behaviour is observed; however, when an accurate solar photon flux is included, a substantial shift in spacecraft potential values is evident in Figure 2, particularly, without the thruster. This difference is attributed to the accurate inclusion of the solar photon flux and associated photoelectron emission.

In contrast, when the thruster is operating a low and stable negative potential is obtained (from -2 V to -6 V) over a wide range of heliocentric distances from 0.067 AU to 1 AU. The primary reason is due to the CEX-ions and the electrons from the cathode dominating the surface and surrounding plasma since their number densities are so much larger, 10^{10} m^{-3} and 10^{11} m^{-3}, respectively (as shown in Figure 3.) The CEX-ions create a dense cloud surrounding the spacecraft which interacts with the charged particles present near the spacecraft. The thruster electrons follow the same path as CEX-ions but with a much higher thermal speed and charging current that leads to a negative charge and potential on the spacecraft. The CEX-ions act as a protective shield between the spacecraft and the surrounding plasma, thereby reducing the impact of ambient electrons. As a result, the operation of an electric thruster provides additional current that controls and stabilizes the spacecraft's potential to a low negative potential. For instance, at 0.067 AU, the spacecraft potential converges to -1.74 V instead of -4.36 V without the thruster. A significant difference in spacecraft potential with and without the thruster (from 0.067 AU to 1AU) is mainly due to the high dominance CEX-ions and thruster electrons that reduce the potential barrier (as shown below in section 3.3) surrounding the spacecraft which no longer restrict the escape of photoelectron and secondaries thus leading to a much less negative potential.

At a distance of 0.044 AU from the Sun, the spacecraft's potential with the thruster is uncertain due to slow and fluctuating convergence. Multiple simulations using the PIC distribution have been performed to assess the spacecraft's potential convergence, which appears to lie within the range of -1 to -3 V. However, as of the present date, the simulations exhibit a significant fluctuation with time and have not yet reached convergence. To check these results, a similar simulation was rerun using the assumption of Maxwell-Boltzmann distributions where thermal electrons are treated as fluid. In this case, the spacecraft's potential lies within the same range of -1 to -3 V, but the convergence is slower, albeit more stable. The sluggish convergence may be due to the high ambient electron and ion temperature and density, which are on the order of 100eV. These factors are likely impeding the attainment of a faster convergence in the PIC and Maxwell-Boltzmann distribution simulations.

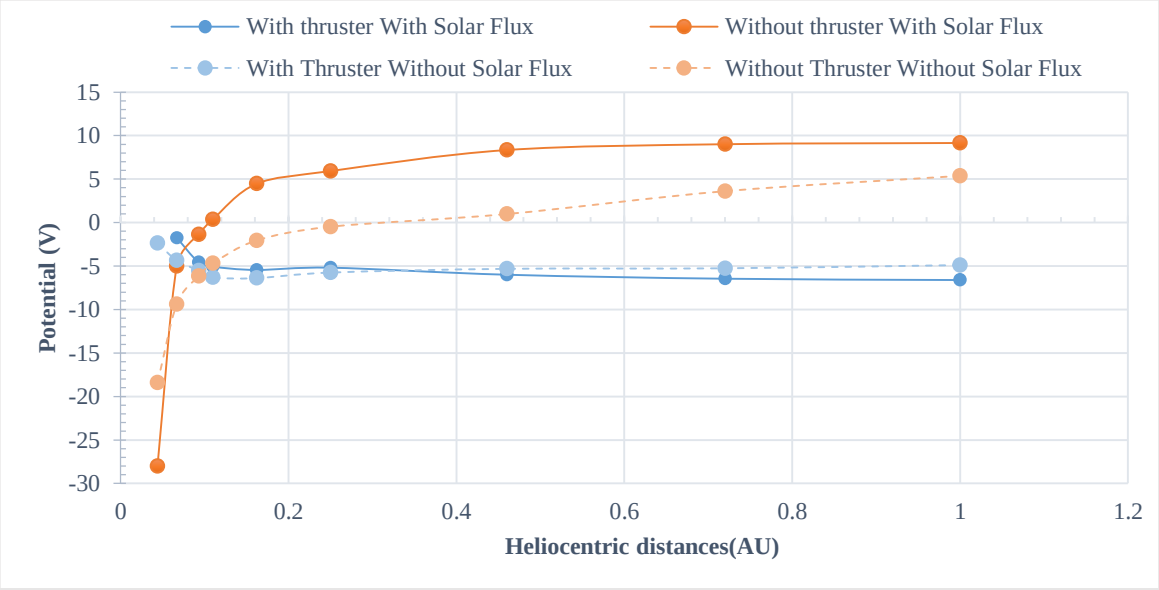

Figure 2. Spacecraft potential variation versus heliocentric distances, with and without thruster, considering Solar Photon Flux (solid orange and blue) and without solar photon flux (dotted Lines).

In our previous paper (Shinde et al., 2023), we achieved qualitatively similar results. However, we considered a constant solar photon flux, leading to an inaccurate spacecraft potential without the thruster, as shown in Figure 2 by the differences between the light orange dotted curve and points (without the correct photon flux) and the solid dark orange lines and points (with the correct photon flux). Interestingly, there were only very small variations in spacecraft potential with the thruster active in Figure 2 for the accurate (dark blue solid curve and points) and constant (light blue dotted curve and points) solar flux cases . Therefore, our current study validates that the solar photon flux doesn't significantly impact spacecraft charging when the thruster is on, in contrast to the scenario without the thruster. It also demonstrates that electric thrusters consistently contribute to reducing and stabilising the spacecraft potential at small negative values across various solar wind conditions, charging it to a low negative potential regardless of solar photon flux.

3.1.1. Fitting Curve

Figures 3a & 3b illustrate the fitting curves for the spacecraft potential versus heliocentric distances. A non-linear Mathematica model is used to fit the curve and estimate the equation for both cases. Equation 6 gives the potential in volts without the thruster on for the simulated spacecraft from 0.044 AU to 1 AU:

$$\Phi = 8.4 - \frac{0.00077}{x^4} + \frac{0.0293}{x^3} - \frac{0.362}{x^2} + \frac{0.542}{x} + 0.623x^2 \quad \text{(V)} \quad . \qquad (6)$$

Here the heliocentric distance x is in the unit of AU. Similarly, Equation 7 predicts the potential of the same spacecraft with the SPT-100 Hall thruster operating for the same geometry from 0.067 AU to 1 AU (0.044 AU is not considered due to the uncertain value of spacecraft potential):

$$\Phi = -6.2 - \frac{0.00002}{x^5} + \frac{0.0009}{x^4} - \frac{0.012}{x^3} + \frac{0.0673}{x^2} - 0.495x^2 \text{ (V)} \quad . \qquad (7)$$

These equations can be used to predict the spacecraft potential at values of *r* that have not been simulated. It's worth noting that while we've simplified the terms, the equations remain a combination of polynomial terms, which are necessary to accurately represent the underlying data and functions over the entire range of distances considered.

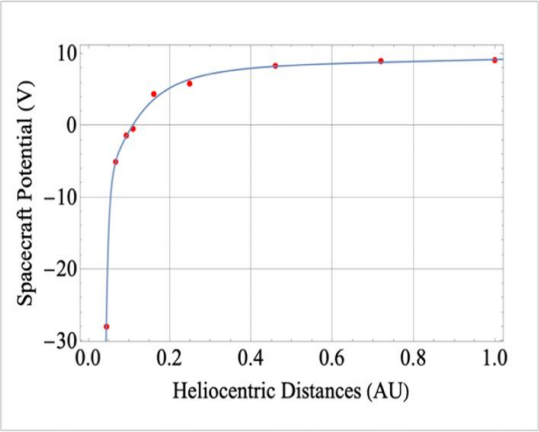

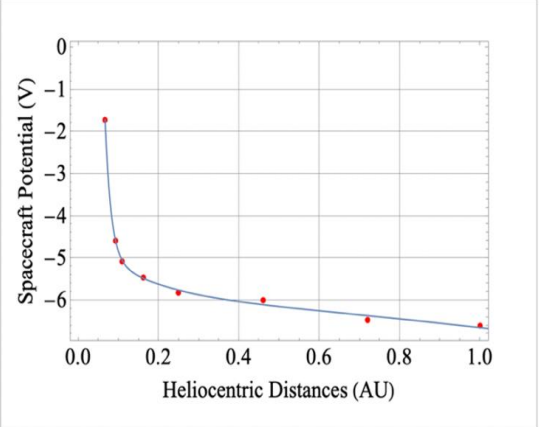

Figure 3. Best-fit curves without and with a thruster vs. heliocentric distance: (Left) 0.044 AU to 1 AU, (right): 0.067 to 1 AU.

3.2. Collected and Emitted currents

Figure 4 shows the collected and emitted currents for the ambient solar wind and thruster particles versus heliocentric distance. The photoelectron, secondary electron, thermal electron and thruster electron currents increase monotonically in magnitude with increasing distance from the Sun from 0.067 AU to 1 AU. On the other hand, it is apparent that the collected CEX-ion current is closely constant for all heliodistances considered. (Note that all currents are considered positive for simplicity). An orange-dotted curve indicates the spacecraft's potential for various heliocentric distances from 0.067 AU to 1 AU. Table 3 provides the main output current values with and without the thrusters for all the simulation cases.

Considering the region further away from the Sun, beyond 0.25 AU, a consistently low and negative potential is observed from 0.25 AU to 1 AU in Figure 4. In this region, the low mean energy of ambient thermal electrons reduces the occurrence of secondary electron emission. The spacecraft surface is primarily influenced by photoelectrons, resulting in positive charging when the thruster is off. However, when the thruster is operated, the positively charged surface becomes enveloped by a dense cloud of CEX-ions, which are associated with higher-speed thruster electrons that are attracted to the positively charged surface. The surface accumulates more thruster electrons to neutralize the positive charge. Since the thermal speed of electrons is much higher than ions the surface collects more negative electrons per unit time, so we often obtain a negative potential when the thruster is on. It is evident from Figure 4 that the collected current of CEX-ion and thruster electrons at 1 AU is about 6.8 mA and 5.7 mA, respectively, which is much higher than the thermal electron current of 0.004 mA. Thus, the thruster backflow plume dominates the solar wind effects in this region.

Between 0.162 AU and 0.093 AU, the dominance of CEX-ions and thruster electrons is much higher than that of thermal electrons. Concurrently, the photoelectron emission and secondary electron emission significantly increase with a smaller distance to the Sun. At the distance of 0.067 AU, the collection current of CEX-ions of about 7.7 mA is slightly higher than the collection current of thermal electrons, which stands at 6.4 mA. Nevertheless, the currents of photoemission and secondary electron emission far exceed that of the thermal electrons. These factors collaboratively contribute to the mitigation of the spacecraft's negative charge. For instance, at 0.067 AU, the spacecraft's negative potential diminishes to a lower value of -1.70 V, as opposed to the value of -5.01 V when the thruster is off. However, it's important to note that the CEX-ions and thruster electron neutralizing effects can lose their validity, if the CEX-ions are smaller than that of the thermal electron collection current. In such a case, the high-energy ambient electrons will dominate the spacecraft, resulting in a substantial negative potential. Notably, the condition at 0.044 AU and 0.025 AU is omitted due to its instability and longer duration to obtain the convergence.

Analysis of Figure 4 shows that from 0.11 AU to 0.067 AU, the thruster electron collection current increases monotonically as the spacecraft approaches the Sun. One possible explanation for this phenomenon is that prior to the thruster's operation, the spacecraft's surface carries a negative charge due to the presence of a high thermal electron density. However, upon thruster activation, the dense cloud of CEX-ions plays a significant role in neutralizing the spacecraft's negative charge. The neutralization occurs primarily by diminishing the strong electrostatic sheath that surrounds the spacecraft. Consequently, photoelectrons and secondary electrons are more prone to escaping from the spacecraft's surface, contributing to the reduction of the negative charge. As a result, the surface tends to attract more of the low-energy thruster electrons in order to attain equilibrium between the emitted and collected currents. The recollection of secondary electrons at 0.067 AU is notably reduced from 12 mA to 5.5 mA, which may result in diminished interference with low plasma measurements. Similarly, the recollection of

photoelectrons at 0.067 AU is reduced from 19 mA to 16 mA. Thus, the study indicates that near-Sun environment, CEX-ions and thruster electrons emitted from the thruster play a crucial role in mitigating the negative charging of the spacecraft. Furthermore, the finding suggests that the CEX-ions and thruster electrons are an crucial parameter in determining the spacecraft's final potential when the thruster is on.

In contrast, in the absence of the thruster, when the spacecraft is far away from the Sun, (beyond 0.25 AU), the main charging factor is photoelectrons, due to the low mean energy of thermal electrons that reduces the rate of secondary electron emission. As shown in Figure 5, at 0.025 AU, the emitted current of photoelectrons is 0.1mA, which is significantly higher than the collected current of thermal electrons at about 0.021 mA. The higher photoemission currents result in a positively charged surface. Moving closer to the Sun, within 0.11 AU, the spacecraft's potential decreases sharply and becomes strongly negative converging to approximately -28 V (at 0.044 AU), despite the presence of high photoelectron and secondary electron emission. As explained in section 3.1 by Ergun et al. (2010) & Guillemant (2013), the electrostatic sheath comes closer to the spacecraft and restricts the escape of photoelectrons and secondary electrons. Due to their insufficient kinetic energy, photoelectrons and secondary electrons do not overcome the strong potential barrier, resulting in high recollection and their return to the spacecraft's surface. The secondary electrons, totalling 38 mA, are recollected back to the spacecraft, leading to the build-up of negative charge. In this scenario, an equilibrium is reached when a significant amount of photoelectron current and secondary electron is collected (Guillemant, 2013). However, the recollection of these low-energy electrons interferes with the measurement of low-energy plasma and contaminates the data. Therefore, having an electric thruster can be beneficial as it provides a stabilizing effect on the spacecraft potential restricting it to small negative values in the range of -2V to -6V and enhances the accuracy of low-plasma measurements, considering that the CEX-ion and thruster electron density is much larger than the ambient density.

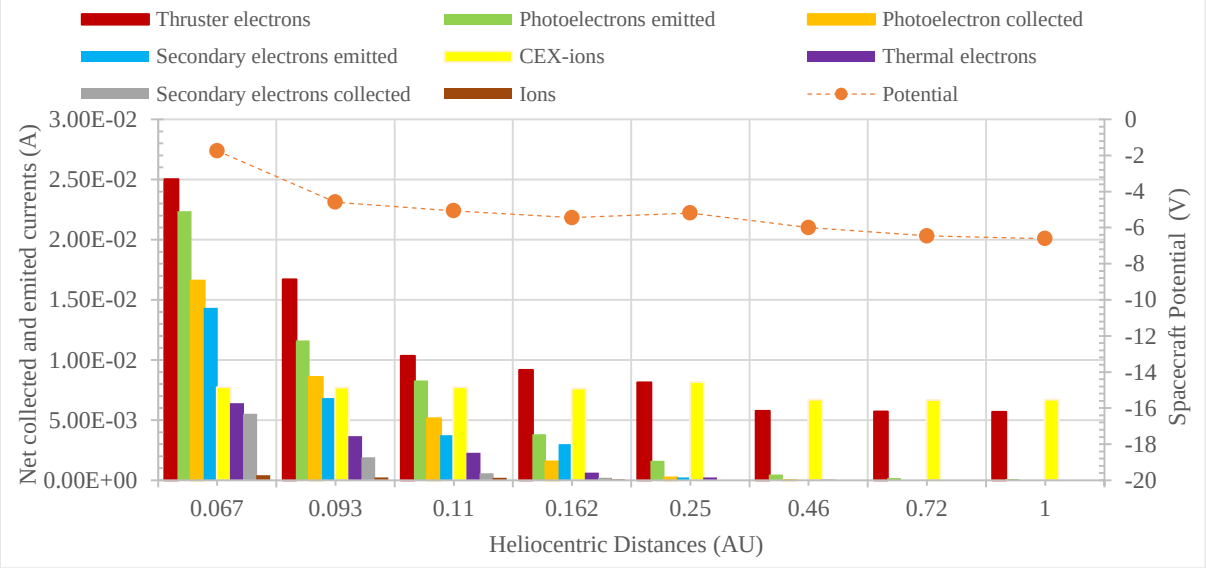

Figure 4. With the thruster on collected and emitted currents (on the primary axis) and spacecraft potential (on the right-hand axis) versus heliocentric distance.

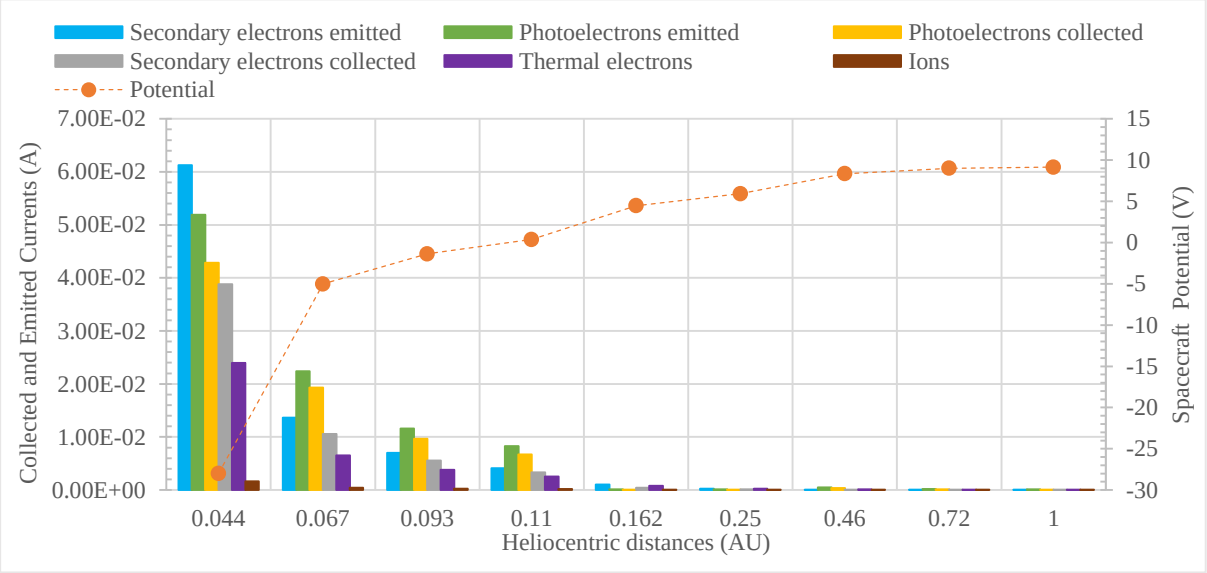

Figure 5. Without the thruster collected and emitted currents (on the primary axis) and spacecraft potential (on the right-hand axis) versus heliocentric distances.

3.3. Ram, Wake, and Side Potential Profiles

Figure 6 demonstrates the intrinsically 2D (rotationally symmetric) nature of the potential structure of the spacecraft which is obtained by cutting Figure 1 along the y=1 plane for varying heliocentric distances. The ram direction is in the negative x-axis direction, and the wake direction is along the positive x-axis. The left images depict the potential with the thruster on from 0.067 AU to 1 AU, while the right-side images show the potential without the thruster activated, for distances from 0.044 AU to 1 AU. The negative potential wells due to photoelectrons and secondary electrons are visible in the ram direction (left side) for all helio distances when the thruster is on and for distances less than 0.25 AU when the thruster is off. In the wake direction the thruster makes the potential positive at all distances, but when the thruster is off a negative well in the potential is visible within about 0.25 AU. This is the standard potential well caused by the exclusion of ambient ions streaming from the Sun by the spacecraft body, whereas the ambient electrons can easily access this region due to their large thermal speeds, making the net charge and potential negative. On the sides (e.g., the +/- z direction) the potential shows a relatively standard sheath. Figure 7 illustrates the evolution of the potential profiles in the ram, wake and -z direction with and without the thruster at various heliocentric distances.

Figures 7a and 7b depict the ram potential, with and without the thruster, in the top left and top right panels, respectively. With the thruster on, as the spacecraft moves from 1 AU to 0.46 AU, it experiences a minimum ram potential near -4 to -5 V, likely due to the accumulation of thruster electrons (Figure 7a). A localized minimum in potential ranging from -7 to -11 V is observed interior to 0.25 AU. The localized minimum can act as a potential barrier or a trap, depending on the particle charge. However, the CEX-ions play a crucial role in neutralizing this potential barrier, maintaining the spacecraft's potential at a more positive value. It is evident from Figure 7a at 0.067 AU, where the potential barrier is reduced from -14 V to -8 V, mainly due to the presence of CEX-ions that help neutralize the charge surrounding the spacecraft. On the other hand, without the thruster, a positive ram potential in the range of 0.6 to 9 V is observed from 1 AU to 0.25 AU (as shown in Figure 7 b). Interior to 0.11 AU, a similar minimum in potential occurs even

when the thruster is inactive, although the potential is much more negative than when the thruster is on. For instance, at 0.067 AU, the potential barrier reaches -14.1 V without the thruster, while it is only -8.3 V with the thruster on. Furthermore, at 0.044 AU, the ram barrier reaches -34 V when the thruster is off, leading to a significant recollection of secondary electrons emitted from the spacecraft. Therefore, the ram potential barriers are substantially reduced when the electric thruster operates near the Sun.

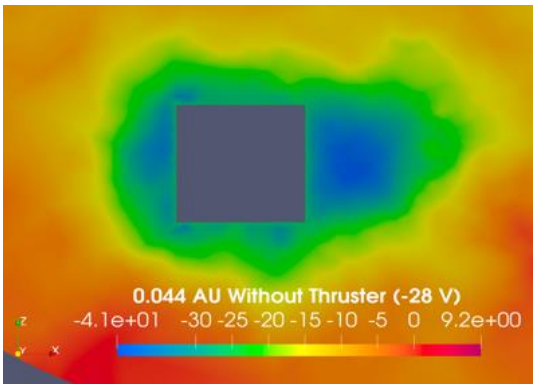

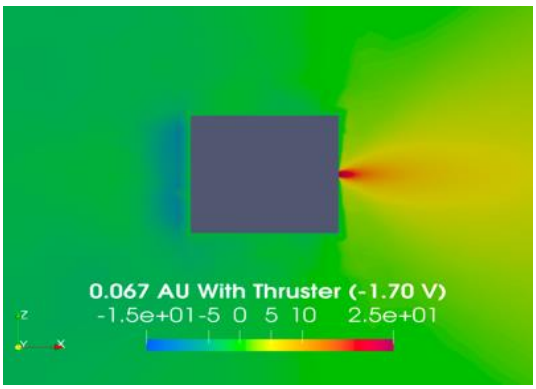

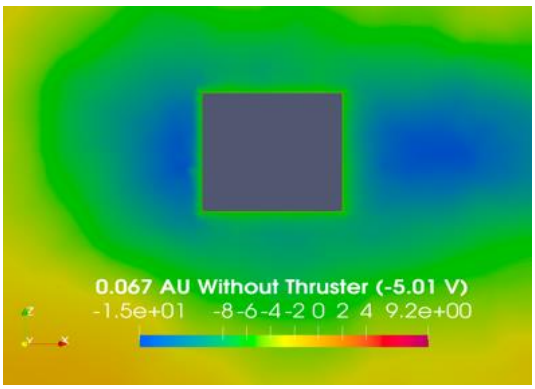

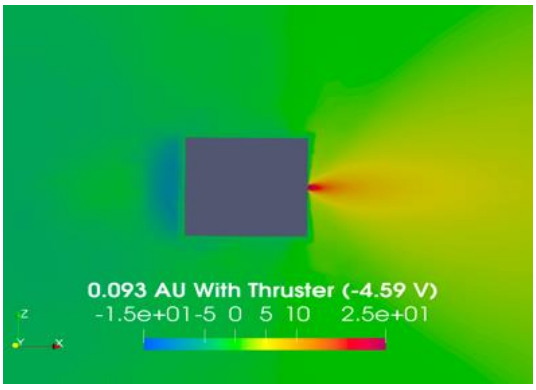

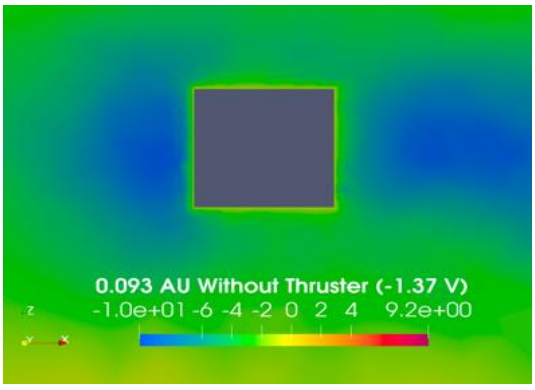

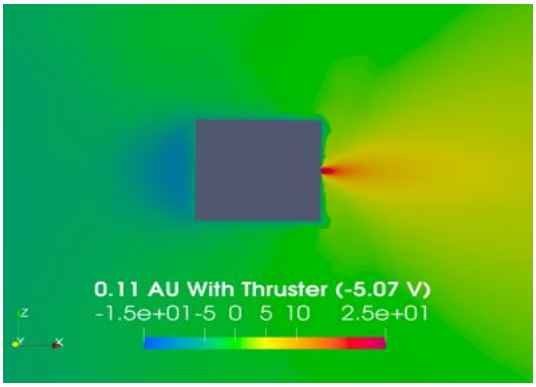
0.11 AU With Thruster (-5.07 V)
-1.5e+01 -5 0 5 10 2.5e+01

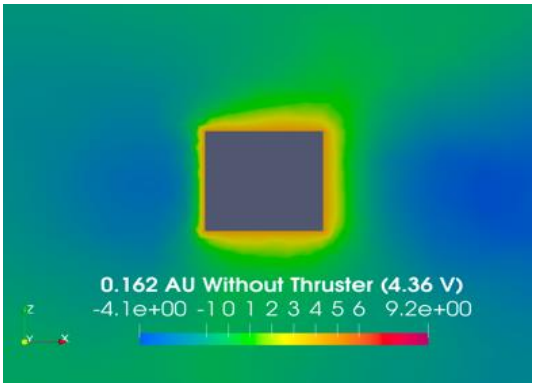
0.162 AU Without Thruster (4.36 V)
-4.1e+00 -1 0 1 2 3 4 5 6 9.2e+00

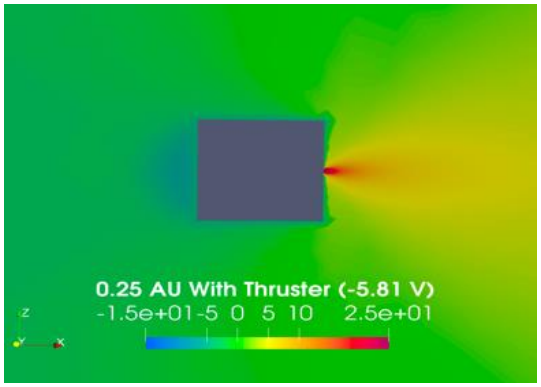
0.25 AU With Thruster (-5.81 V)
-1.5e+01 -5 0 5 10 2.5e+01

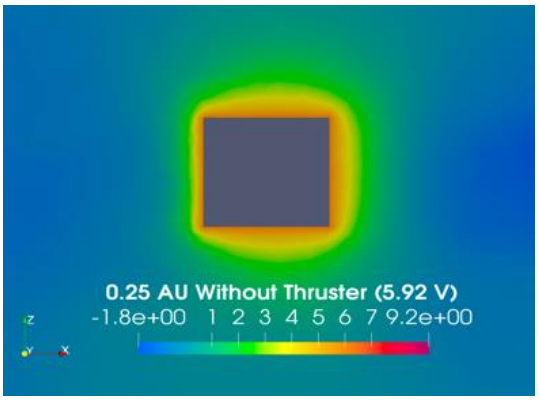
0.25 AU Without Thruster (5.92 V)
-1.8e+00 1 2 3 4 5 6 7 9.2e+00

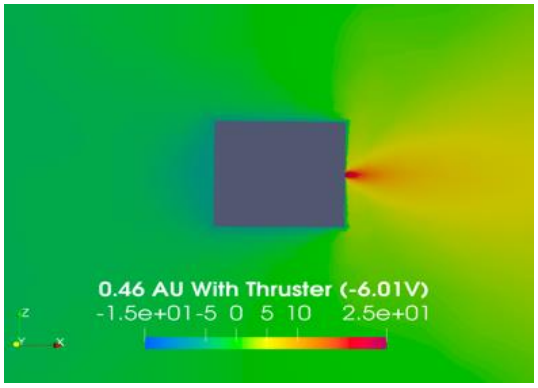
0.46 AU With Thruster (-6.01V)
-1.5e+01 -5 0 5 10 2.5e+01

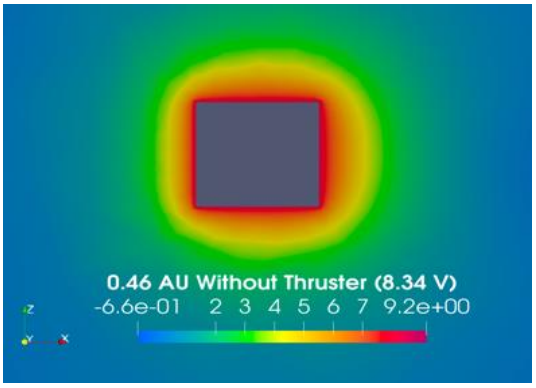
0.46 AU Without Thruster (8.34 V)
-6.6e-01 2 3 4 5 6 7 9.2e+00

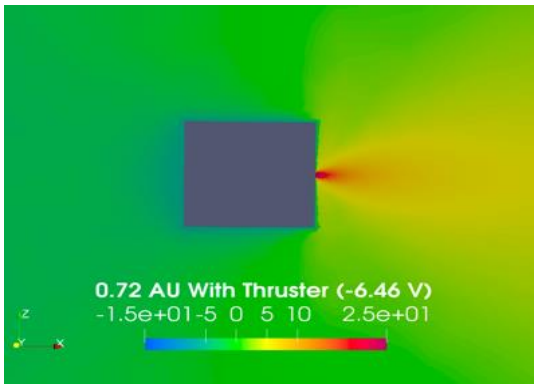
0.72 AU With Thruster (-6.46 V)
-1.5e+01 -5 0 5 10 2.5e+01

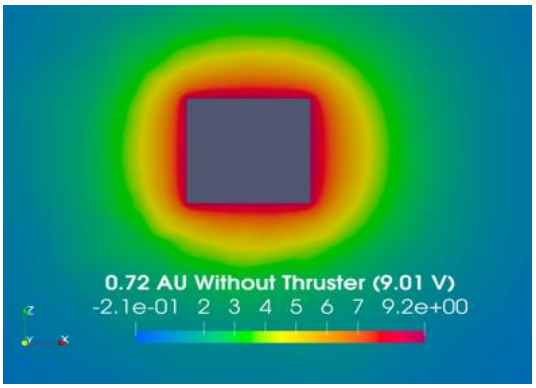
0.72 AU Without Thruster (9.01 V)
-2.1e-01 2 3 4 5 6 7 9.2e+00

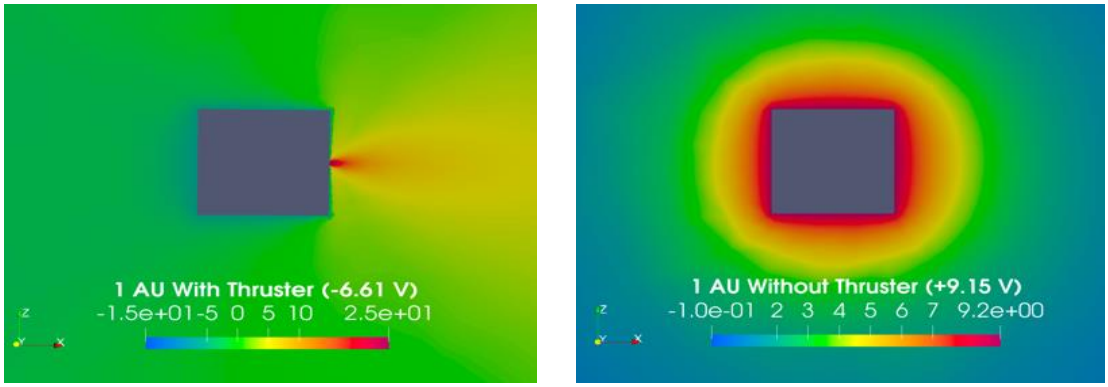

Figure 6. Cross comparisons of 2D potential maps with and without the SPT-100 Hall thruster on at varying heliocentric distances, corresponding to Figure 1 and the 3D potential cut in the y = 1 plane. Sunlight and the solar wind come from the left (the -x direction).

Figures 7c and 7d show the wake potential structure with and without the thruster in the middle left and middle right panels, respectively. A stable positive potential of approximately +25 V is observed at the satellite when the thruster is on, with the potential decreasing monotonically with increasing distances from the spacecraft (Figure 7c). Note that the potential profiles are essentially independent of helio distance when the thruster is on, consistent with the thruster plume dominating all other charging influences. Taken together, the wake region behind the spacecraft is filled with ions and electrons emitted from the thruster. As a result, it develops a plasma sheath which acts as a barrier to ambient electrons directly impacting the spacecraft's surface. The sheath's reduction of potential with increasing distance into the plasma is primarily due to larger electron densities. Overall, the presence of positive ions in the wake of an electric thruster can play a significant role in reducing spacecraft charging and managing potential barriers, contributing to the safe and stable operation of the spacecraft in the space environment. On the other hand, without the thruster on (Figure 7d), the wake potentials at and above 0.25AU decrease monotonically with increasing distance from the spacecraft. However, interior to 0.162 AU the profile develops a localized minimum near x = 1 m with a magnitude that increases as the heliocentric distance decreases. For instance, at 0.067 AU this wake barrier reaches -14 V when the thruster is off. As we go further towards the Sun at 0.044 AU, the wake barrier reaches -40 V which may result in the return of low-energy electrons back to the surface and enhancing spacecraft charging dynamics. Thus, when the thruster is off the spatial profiles of the potential in the ram and wake directions are surprisingly similar, presumably because of increased electron densities due to increased photoelectron effects (ram direction) and hotter, denser, ambient electrons in the wake cavity, respectively.

Figures 7e and 7f show the sheath profiles (perpendicular to the ram and wake axis) with and without the thruster in the bottom left and bottom right panels, respectively. Figure 7e shows a low, negative potential in a small range of -2 to -6 V from 0.067 AU to 1 AU with the thruster on compared to Figure 7f having a large range of -40 to +9 V with the thruster off from 0.044 AU to 1 AU, respectively. With the thruster on the spatial profiles are reminiscent of a standard sheath for cold dense electrons (small Debye length) about a negative potential object for R > 0.093 AU. Similarly, for R > 0.093 AU and the thruster off the monotonic potential profile appears appropriate for a standard sheath about a positively charged object for warm dilute electrons (large Debye length). Only for R< 0.093 AU do the perpendicular sheaths change character and evolve towards having a negative potential well when the thruster is off. Note that the satellite potentials are the same in the ram and z directions (Figures 7a, 7b, 7e and 7f), as expected for a conducting spacecraft surface, and that the potential in the wake direction (Figure 7c) is different due to the thruster and satellite surface being isolated by a resistor.

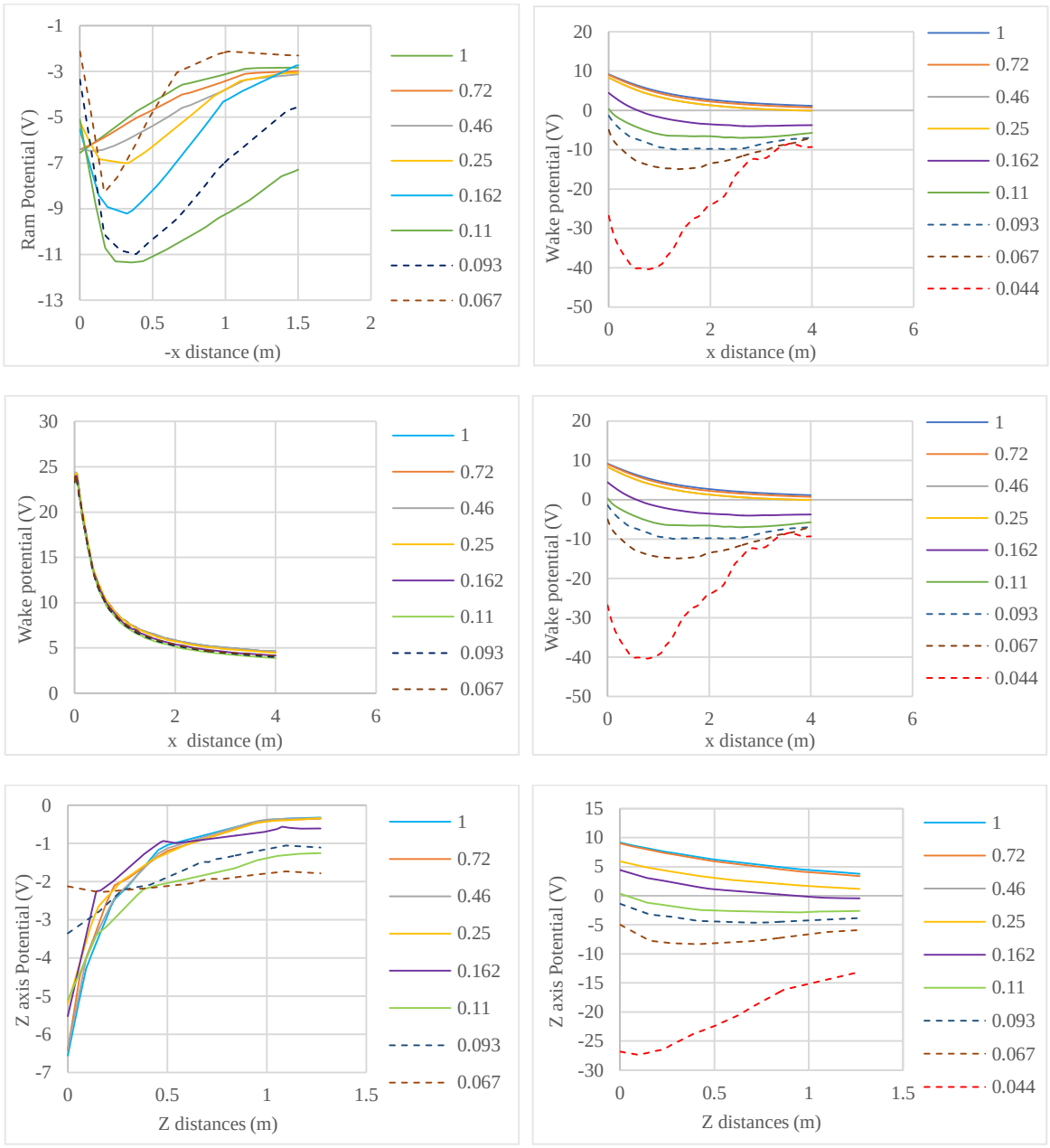

Figure 7. The potential profiles along the ram direction (-x axis), wake direction (x-axis) and the sheath direction (z-axis), obtained from Figure 6.

3.4. With and Without the Thruster: Role of Secondary Electrons

Figure 8 illustrates the impact of secondary electrons on the spacecraft potential at distances of 0.067 AU and 1 AU with and without the thruster. It is apparent from Figure 8a that at 1 AU, the influence of secondary electrons on the spacecraft potential is negligible, while at 0.067 AU, there is a significant variation when the thruster is on. As expected, the inclusion of secondary electrons leads to the satellite potential becoming more positive. On the other hand, without the thruster from Figure 8b, it is evident that secondary electrons have a greater influence on spacecraft potential at 0.067 AU than at 1 AU. Figures 9a and 9b display the collected and emitted current with the thruster at 0.067 AU in the top left and 1 AU in the top right, respectively. Meanwhile, Figures 9c and 9d depict the collected and emitted current without the thruster at 1 AU in the bottom left and 1 AU in the bottom right, respectively.

The emission of secondary electrons during thruster operation depends on both ambient and thruster electrons impacting the spacecraft. In Figure 8a (right) at 0.067 AU when the thruster is on, the spacecraft charges to -3.5 V instead of -1.74 V. A detailed analysis, as shown in Figure 9a, reveals that the collection of thruster electrons greatly increases from 25 mA to 200 mA when the secondaries are eliminated, while the thermal electron collection current decreases from 6.9 mA to 2.1 mA, reducing the return of photoelectrons current from 18 mA to 3.8 mA. The sudden increase in thruster electron current is likely attributed to the reduction in spacecraft potential and secondary electrons, leading to a reduction in thermal electron current. The negatively charged surface attracts CEX-ions, causing a slight rise in their current from 7 mA to 10 mA. With the combined effects of CEX-ions and photoelectron emission, the negative spacecraft potential diminishes, resulting in a greater accumulation of thruster electrons. Consequently, the spacecraft becomes charged to a slightly higher negative potential, approximately -3.1 V instead of -1.7 V. It's important to note that despite the substantial current collection of the thruster electron the spacecraft does not excessively charge the spacecraft to a highly negative potential due relatively low temperature of thruster electrons (0.5 eV) in comparison to ambient electrons or any other currents. In conclusion, in the near-Sun environment, the emission of secondary electrons has a significant influence on the spacecraft and surrounding plasma potentials during thruster operation.

On the other hand, at 1 AU, when the thruster is active, there is a negligible difference in spacecraft potential with or without secondaries. The spacecraft charges to -4.9 V (without secondaries) instead of -4.8 V (with secondary electrons), as shown in Figure 8a (right). In this case, the low-density thermal electrons from the ambient plasma are dominated by the CEX-ions and thruster electrons (Figure 9b). The low mean energy of thermal electrons decreases the rate of secondary electron emission, allowing the CEX-ions and thruster electrons to dominate the spacecraft and the surrounding plasma. Since the solar photon flux is reduced at 1 AU, the effect of photoelectrons on spacecraft charging is negligible, as will be explained in detail in the next section 3.5. From Figure 9b, it is evident that the collected current of thermal electrons and photoelectrons is much lower than the currents of thruster electrons and CEX-ions, both with and without secondaries. Hence, secondary electrons are less important and do not significantly affect the spacecraft's potential when far away from the Sun.

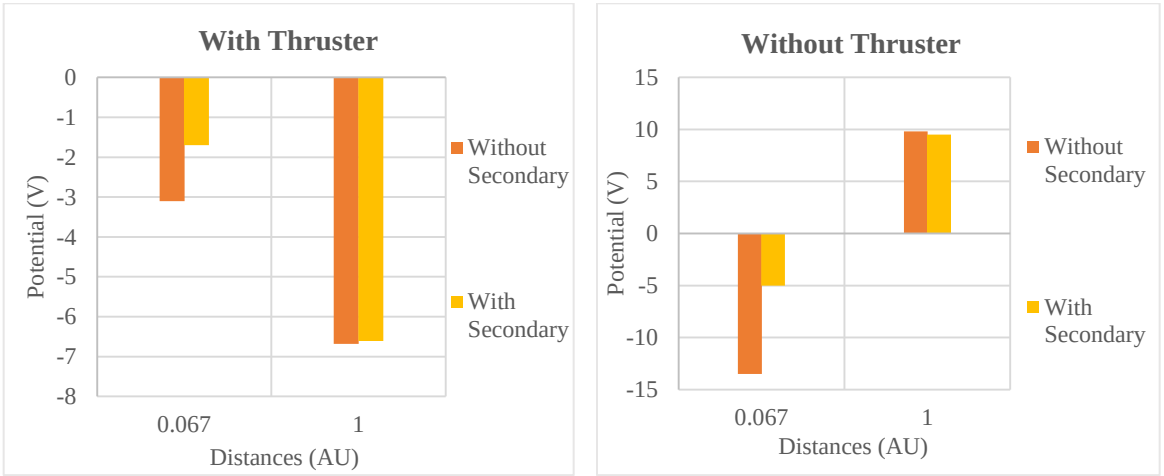

Figure 8. Spacecraft potential with and without secondary electrons at 1 AU and 0.067 AU, from left to right: a.) with the thruster and b.) without the thruster.

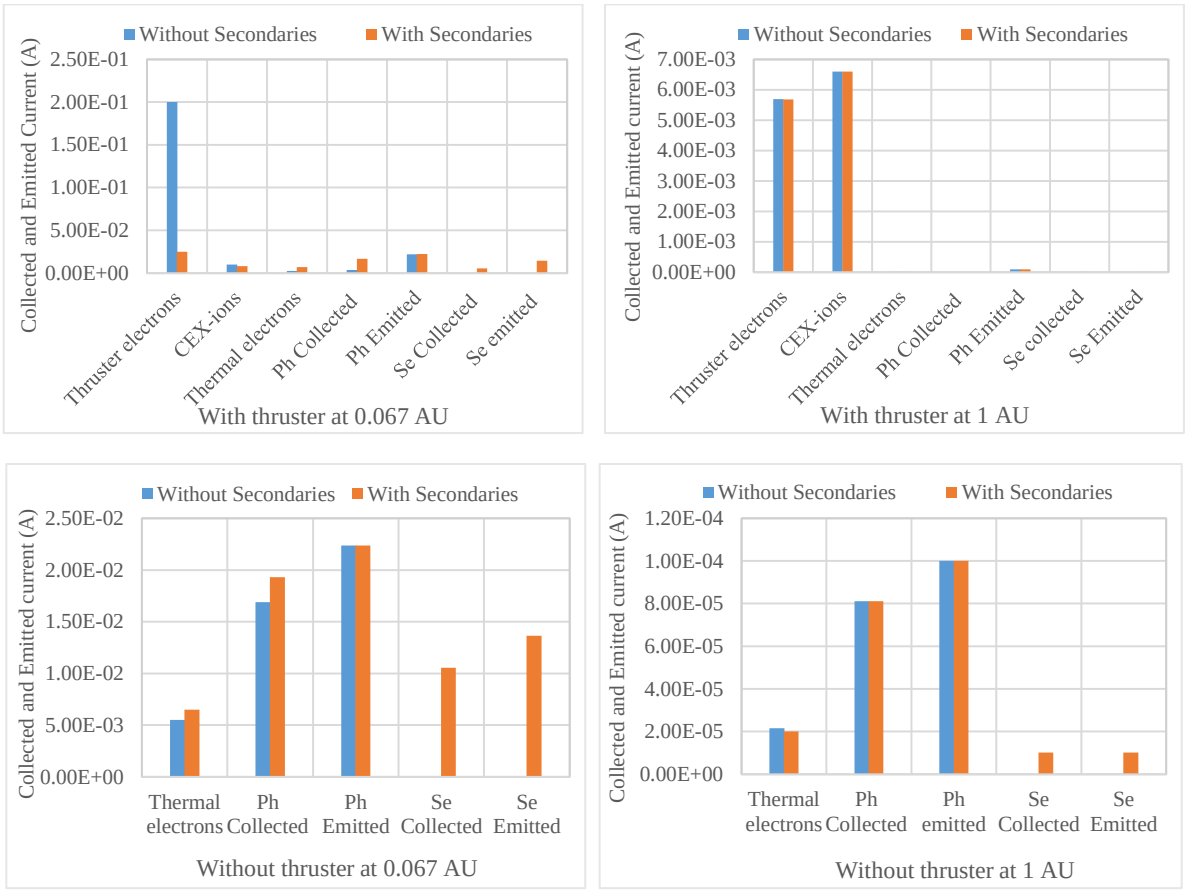

Figure 9. Collected and emitted currents with and without the thruster at 0.067 AU and 1 AU. From top left to bottom right, respectively: a.) With the thruster at 0.067 AU, b.) With the thruster at 1AU, c.) Without the thruster at 0.067 AU, and.) Without the thruster at 1AU.

In Figure 9c, at 0.067 AU without the thruster, minor variations in the collection of thermal electron and photoelectron currents are noticeable. However, at 1 AU (Figure 9d), the currents remain consistent whether secondaries are present or not. When the thruster is off, at 0.067 AU, the spacecraft potential has a significantly more negative value of -13.1 V instead of -5.01 V due to the high dominance of thermal electrons (as shown in Figure 8b). Since secondary electrons are not present, there is no potential barrier which results in a much higher ram potential of -16.3 V and wake potential of -23.6 V. The absence of secondary electrons reduces the collected current of thermal electrons from 7 mA to 5.5 mA and photoelectron current from 18 mA to 13 mA (as shown in Figure 9 c). The emitted photoemission current is constant regardless of the presence or absence of secondaries. In such cases, the surface accumulates high-temperature ambient electrons with zero emission leading to a large negative potential. Thus, in the vicinity of the Sun at 0.067 AU, secondary electrons play a crucial role in reducing the negative potential of the satellite when the thruster is off. In contrast, at 1 AU, without the thruster, the elimination of secondary electrons has a negligible impact on spacecraft potential due to the low mean energy of thermal electrons (as shown in Figure 8b). From Figure 9d, it is evident that the collected and emitted currents at 1 AU are constant with or without secondary electrons.

In summary, the findings suggest that the secondary electrons significantly help to mitigate the spacecraft's negative charge in close proximity to the Sun, irrespective of whether the thruster is on or off. Indeed, the absence of secondary electrons makes the spacecraft's potential more negative when the thruster is on, albeit to a significantly lesser degree than in the absence of the thruster and secondary electrons. In contrast, the impact of secondary electrons on the spacecraft potential is negligible near the Earth (relatively far away from the Sun) irrespective of the thruster being on or off.

3.5. With and Without the Thruster: Role of Photoelectrons

Figure 10 shows the effect of photoelectrons on the spacecraft potential at distances of 0.067 AU and 1 AU, both in the presence and absence of the thruster. As shown in Figure 10a, when the thruster is on, the influence of photoelectrons on spacecraft potential at 1 AU is negligible. However, at 0.067 AU, Figure 10a demonstrates a noticeable factor of 2 variations in the spacecraft potential. The spacecraft at 0.067 AU charges to -4.45 V instead of -1.70 V. The possible explanation is similar to the case without secondary electrons discussed in Section 3.4, where the high-density CEX-ions and thruster electrons dominate the plasma and the spacecraft environment, diminishing the importance of photoelectrons. Figure 10b when the thruster is off, further highlights the significant impact of photoemission on spacecraft potential at both the location at 1 AU and 0.067 AU. As expected, the inclusion of photoelectrons leads to a more positive spacecraft potential at both distances and when the thruster is on or off. Figures 11a and 11b display the collected and emitted current with the thruster at 0.067 AU in the top left and 1 AU in the top right, respectively. Meanwhile, Figures 11c and 11d depict the collected and emitted current without the thruster at 1 AU in the bottom left and 1 AU in the bottom right, respectively.

From Figure 11a, it is evident that at 0.067 AU with the thruster, the collected current of thermal electrons and CEX-ions remains constant with or without photoemission. However, a decrease in thruster electron current is observed from 25 mA to 13 mA when photoelectrons are neglected. And potential becomes more negative. One possible reason could be that the spacecraft is exposed to a hot and dense environment, resulting in the penetration of the surface by high-temperature thermal electrons (few 10 to 100 eV). Consequently, it leads to a high secondary electron emission that helps to take away the negative charge. Similarly, the CEX-ions contribute significantly to reducing the negative potential of the spacecraft. However, due to the relatively high temperature of the thermal electrons compared with other charged particles, the spacecraft tends to settle at a negative potential and thus repels the thruster electrons. As a result, thruster electron accumulation on the surface is dependent on photoelectron and secondary electron emission. From Figure 11b it is clear that at 1 AU, the thruster electrons and CEX-ions dominate the photoelectron effect and have negligible impact on spacecraft potential irrespective of the presence or absence of photoemission.

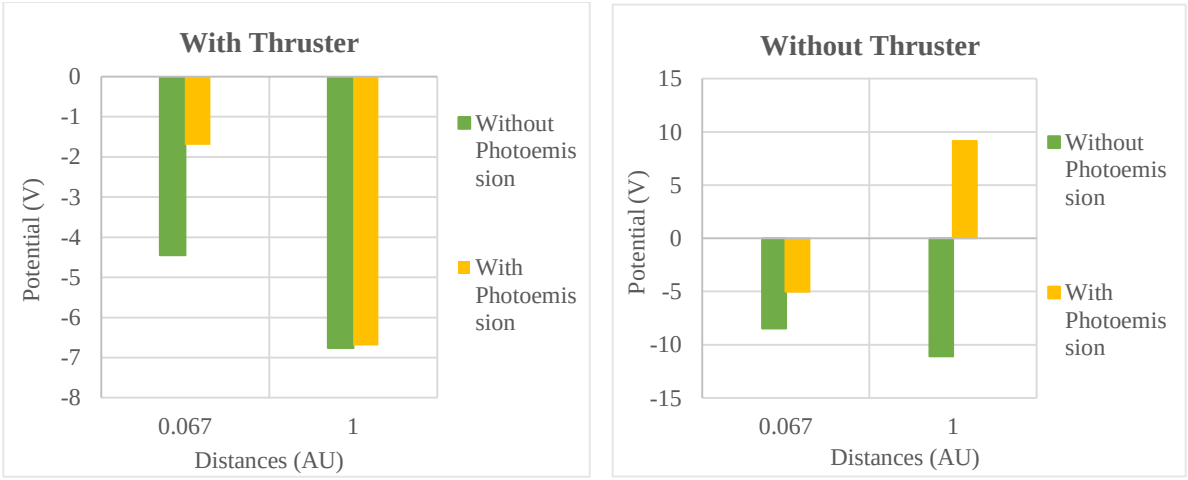

Figure 10. Spacecraft potential with and without photoelectrons at 1 AU and 0.067 AU, from left to right: a.) with the thruster on and b.) without the thruster

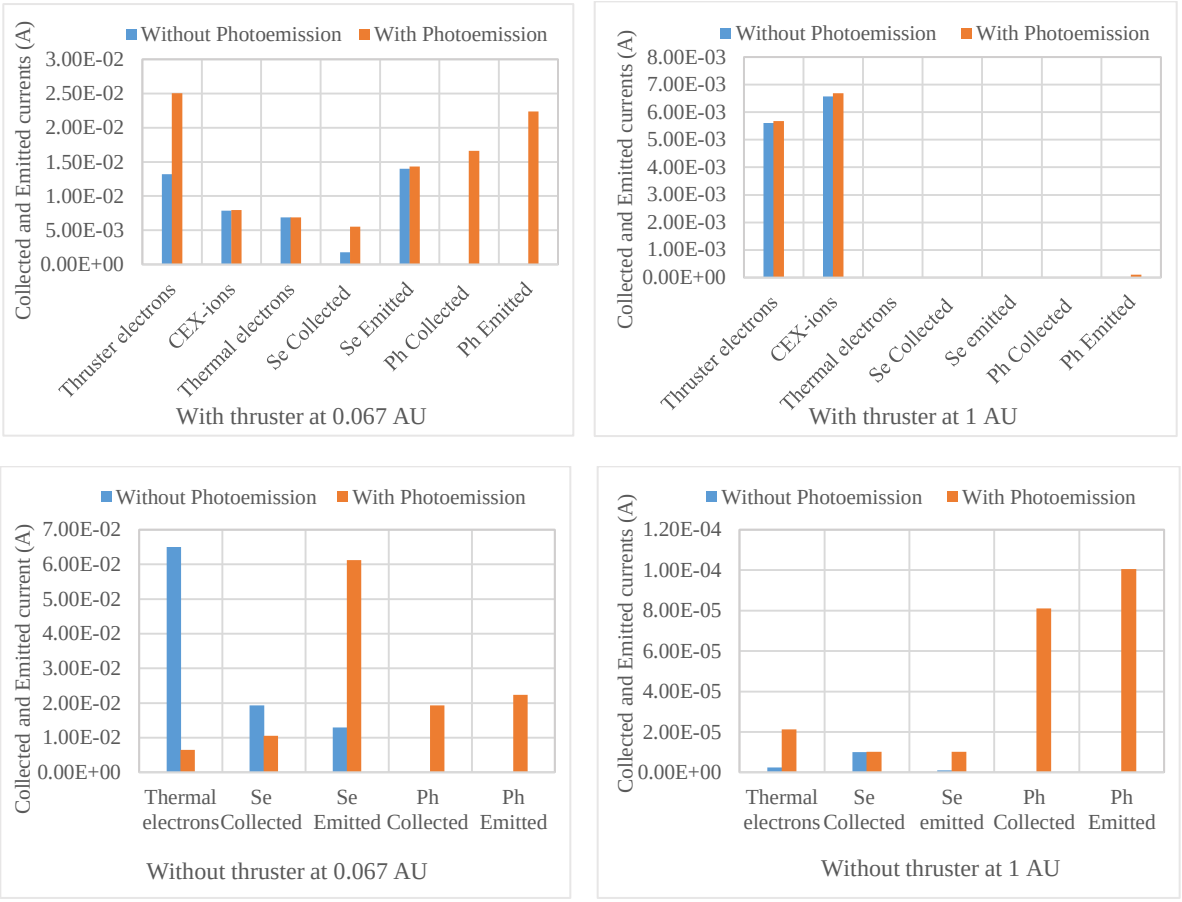

Figure 11. Collected and emitted currents with and without the thruster at 0.067 AU and 1 AU. From top left to bottom right, respectively: With the thruster at (a) 0.067 AU, and (b) 1AU and without the thruster at (c) 0.067 AU and (d) 1AU.

Moving to the scenario without the thruster, from Figure 11c it is clear that eliminating photoemission at 0.067 AU and 1 AU leads to a significant variation in spacecraft potential. In both cases, the photoelectric effects are important and make the spacecraft significantly positive. Indeed at 1 AU a significant change in spacecraft potential is seen from -11 V to + 9V when photoelectrons are included. While at 0.067 AU, the spacecraft potential without photoemission is -8.4 V instead of -5.01 V (as shown in Figure 10b). Close to the Sun, photoemission is quite strong, but it has a minor effect on making the spacecraft positive. The seemingly contradictory result is explained in section 3.1, in terms of the high density of thermal electrons generating a strong potential barrier that hinders the escape of photoelectrons and secondary electrons, leading to a significant accumulation of electrons on the spacecraft's surface. The same can be observed in Figure 11c, where the thermal electron collected current on the surface increases from 6.5 mA to 65 mA. In such a situation, the return of the secondary electron increases from 10 mA to 19 mA, and the emission rate is significantly lowered from 61 mA to 13 mA without photoemission. Thus, close to the Sun at 0.067 AU, despite its high solar photon flux, the spacecraft charges to a negative potential, and in the absence of photoemission, its potential becomes more negative.

Conversely, at 1 AU without the thruster, the spacecraft potential in the absence of photoemission converges to -11.1 V instead of +9 V (as shown in Figure 10b). At this distance, photoemission is the primary charging factor that causes the spacecraft to become positively charged, due to the low density of thermal electrons. However, in the absence of sunlight the thermal electrons tend to accumulate on the spacecraft, leading to a large negative potential. From Figure 11d, it is evident that the lack of

photoelectrons results in a substantial decrease in the collected current of thermal electrons, due to a strong build-up of the negative charge that repels the incoming electrons. On the other hand, in the presence of photoemission, the current of photoelectrons dominates the thermal electron current by a factor of 10, making the spacecraft charge positively and leading to the attraction of thermal electrons.

In summary, the simulations show that photoemission plays a pivotal role in mitigating the negative charge of the spacecraft close to the Sun, irrespective of whether the thruster is on or off. Indeed, the absence of photoemission impacts the spacecraft's potential when the thruster is on, albeit to a significantly lesser degree than in the absence of the thruster and photoemission. For example, at a distance of 0.067 AU, with the thruster but without photoemission, the spacecraft's charges at -4.45 V, while without both the thruster and photoemission, the spacecraft's potential converges to a higher negative value of -8.47 V. Similarly, when situated far from the Sun at 1 AU, the spacecraft's potential without the thruster and without photoemission reaches a substantial negative value of -11.1 V. In contrast, with the thruster but without photoemission, the potential stabilizes at -6.7 V. As such, the roles of CEX-ions and thruster electrons are essential in maintaining a low negative potential in the absence of photoemission, both at the location of 0.067 AU and 1 AU.

3.6 With the Thruster: Without Secondaries and Photoemission

Figure 12 illustrates the impact of eliminating simultaneously secondaries and photoelectrons on spacecraft potential at 0.067 AU and at 1 AU. The results specifically focus on the thruster's operation and do not include a scenario without the thruster, as the primary objective is to understand spacecraft charging during thruster operation. In this scenario, the photoelectrons and secondary electrons are both eliminated at 0.067 AU, and the spacecraft charges to a significantly higher negative potential of -11.1 V instead of -1.7 V, despite the presence of high-density CEX-ions and thruster electrons. This is in contrast to -3.1 V without secondaries only and -4.5 V without photoemission only (from sections 3.5 and 3.6). Thus, the combined absence of photoelectrons and secondary electrons can lead to high negative charging of the spacecarft. The large negative charging can be explained by the fact that the spacecraft, being exposed to a hot and dense environment, experiences significant charging by high-temperature thermal electrons (few 10 to 100 eV). The absence of photoemission and secondary electrons prevents the removal of electrons from the surface, resulting in a large negative potential. Since the thermal electron temperature is so high compared to the energies of any other particles it controls the spacecraft potential. The combined elimination of secondary electrons and photoemission causes the spacecraft to charge to a large negative potential. The CEX-ions and thruster electrons compensate if either of them is not present and charges the spacecraft to a much less negative potential (as shown in section 3.4 and 3.6). Hence in order to achieve equilibrium, the incoming ambient electron current must be equal to that for the net photoelectrons, secondary electrons, CEX-ions and thruster electrons. Figure 12a clearly demonstrates that the collected current of thruster electrons is significantly reduced from 25 mA to 1.8 mA due to the repulsion caused by the strongly negative surface potential when secondaries and photoemission are not included. Thus, the presence of photoelectrons and secondary electrons is crucial in maintaining a smaller magnitude of negative potential when the thruster is active. The absence of either one may not have a significant impact, but their combined elimination can result in excessive negative charging of the spacecraft.

On the other hand, Figure 12b shows that the simultaneous elimination of secondary and photoelectrons at 1 AU has a negligible effect on spacecraft potential, owing to the decreased energy and density of thermal electrons. The final spacecraft potential at 1 AU converges to -6.75 V, only very slightly different from the potential of -6.72 V. In summary, at 0.067 AU, photoelectrons and secondary electrons play a vital role in preventing excessive negative potential, while the absence of either one may have a significant but smaller impact on the spacecraft potential. However, at 1 AU, the simultaneous elimination of photoelectrons and secondary electrons shows negligible effects on spacecraft potential when the thruster is active.

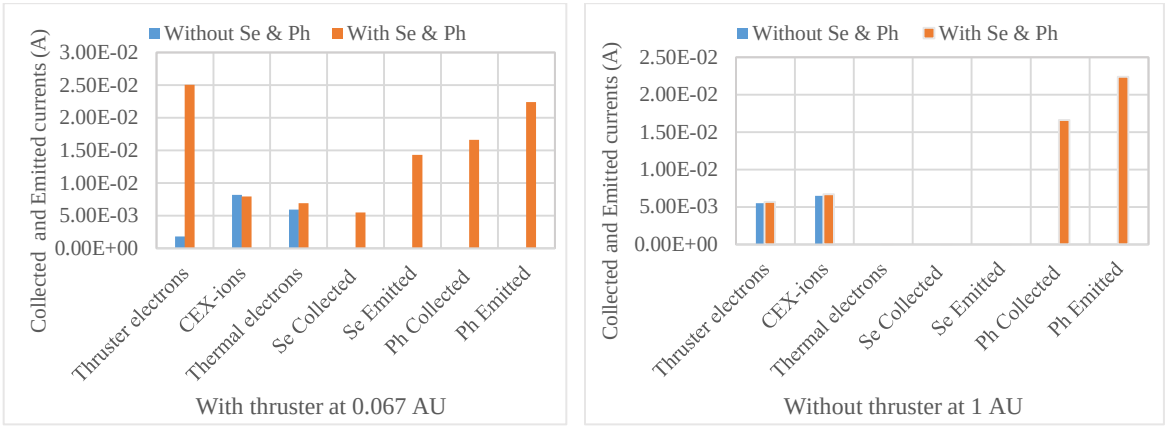

Figure 12. Collected and emitted currents with the thruster on but no photoemission and secondary electrons at (a.) 0.067 AU and b.) 1 AU.

Table 3

SPIS Simulation Main Output Values With And Without Thruster For Various Heliocentric Distances

Heliocentric Distances (AU)	**1**	**0.72**	**0.46**	**0.25**	**0.162**	**0.11**	**0.093**	**0.067**	**0.044**
				WITH THRUSTER					
Current (A)									
Thermal electrons	-4.0e-6	-1.0e-5	9.4e-6	-2.4e-4	-6.2e-04	-2.2e-3	-3.6e-3	-6.9e-3	-
Ions	1.8e-6	3.5e-6	-4.4e-5	3.2e-5	7.6e-5	1.97e-4	2.4e-4	4.1e-4	-
Photoelectrons									
Collected	-1e-8	-1e-8	-2.0e-7	-2.4e-4	-1.5e-3	-5.16e-3	-8.5e-3	-1.8e-2	-
Emitted	1e-4	1.9e-4	4.7e-4	1.6e-3	3.8e-3	8.3e-3	1.1e-2	2.2e-2	
Net	9.9e-5	1.8e-4	4.6e-4	1.36e-3	2.3e-3	3.14e-3	2.5e-3	4e-3	
Secondaries									
Collected	-1.9e-8	-8.0e-9	-1.7e-9	-1.9e-5	-2.2e-4	-5.7e-4	-1.9e-03	-5.5e-3	-
Emitted	1.4e-6	4.6e-6	3.1e-5	2.4e-4	8.4e-4	3.7e-3	6.8e-3	1.4e-2	
Net	1.4e-6	4.5e-6	3.0e-5	2.21e-4	6.2e-4	3.16e-3	4.9e-3	8.5e-3	
Thruster electrons	-5.6e-3	-5.7e-3	-5.7e-3	-8.1e-03	-9.1e-03	-1.0e-2	-1.6e-02	-2.5e-02	-
CEX-ions	6.6e-3	6.6e-3	6.7e-3	8.1e-03	7.6e-03	7.7e-3	7.7e-03	7.9e-03	-
All Populations									

Collected	-7.5e-6	-1.40e-5	-2.9e-5	-9.7e-5	-2.5e-4	-6.09e-4	-2.8e-3	-2.8e-4	-
Emitted	-7.0e-6	-1.0e-5	-2.5e-5	-9.4e-5	-2.5e-4	-6.03e-4	-2.6e-3	-1.9e-4	
Net	-2.5e-6	-3.9e-6	-3.8e-6	-2.4e-6	-1.5e-6	-6.31e-6	-1.5e-4	-4.7e-4	
Potential (V)									
Spacecraft potential	-6.61	-6.46	-6.0	-5.19	-5.45	-5.07	-4.59	-1.74	-
				WITHOUT THRUSTER					
Thermal	-2.1e-5	-4.0e-5	-1.0e-4	-2.7e-4	-7.9e-4	-2.5e-3	-3.7e-3	-6.5e-3	-2.4e-2
Ions	1.6e-6	3.2e-6	8.5e-6	2.9e-5	7.34e-5	1.8e-4	2.5e-4	4.50e-4	1.67e-3
Photoelectrons									
Collected	-8.1e-5	-1.5e-4	-3.7e-4	-1.6e-5	-1.2e-5	-6.7e-3	-9.6e-3	-1.9e-2	-4.2e-2
Emitted	1e-4	1.9e-4	4.7e-4	1e-4	1e-4	8.3e-3	1.1e-2	2.2e-2	5.1e-2
Net	2e-5	4e-5	1e-4	8.4e-5	8.8e-5	1.6e-3	1.4e-3	3e-3	9e-3
Secondaries									
Collected	-1.1e-5	-2.5e-5	-7.5e-5	-1.2e-5	-4.2e-4	-3.3e-3	-5.5e-3	-1e-2	-3.8e-2
Emitted	1.4e-5	3.1e-5	7.8e-5	2.7e-4	1e-3	4.1e-3	7.0e-3	1.3e-2	6.1e-2
Net	3e-6	6e-6	3e-6	2.5e-4	5.8e-4	8e-4	1.5e-3	3e-3	2.30e-2
All Populations									
Collected	-9.9e-5	-1.93e-4	-4.95e-4	-7.46e-4	-7.86e-4	-1.12e-2	-9.28e-3	-8.88e-3	-9.91e-2
Emitted	-9.9e-5	-194e-4	-4.96e-4	-7.46e-4	-7.85e-4	-1.13e-2	-9.22e-3	-8.92e-3	-1.0e-1
Net	-2.5e-7	4.93e-7	1.28e-6	4.83e-6	-6.07e-7	1.77e-5	-5.93e-5	4.16e-5	9.30e-3
Potential (V)									
Spacecraft potential	9.15	9.01	8.34	5.92	4.46	0.37	-1.37	-5.01	-28

4. Conclusion

The study investigated the effects of spacecraft charging induced by the operation of the SPT-100 Hall thruster in various space environments, ranging from 0.067 AU to 1 AU. The analysis considered factors such as ambient electrons and ions, CEX-ions and thruster electrons, photoelectrons, secondary electrons, and solar photon flux. The results revealed significant variations in space charge and potential barriers when comparing thruster-on and thruster-off scenarios. During thruster operation, the spacecraft potential tends to settle at a low, stable and negative potential, ranging from -2 V to -6 V from 0.067 AU to 1 AU, respectively. The low negative potential is primarily attributed to the presence of thruster electrons and high-density CEX-ions, which dominate the in situ plasma. In contrast, without the thruster, the spacecraft potential exhibited a wide range from 0.044 A to 1 AU spanning from -28 V to +9V, respectively. The spacecraft potential without the thruster is primarily influenced by the increasing energy and number density of thermal electrons and increasing roles of photoelectrons and secondary electrons as the spacecraft approaches closer to the Sun. It's crucial to emphasize that the stabilizing effect of the thruster, particularly in relation to maintaining a low negative potential, relies on factors such as the density of charge-exchange ions (CEX-ions), thruster electron, the ambient electron density, photoelectrons, secondary electrons and the spacecraft's geometry. Above all, the finding of this paper suggests that under various conditions, the SPT-100 Hall thruster can effectively maintain and stabilize the spacecraft potential, mainly due to the influence of high-density CEX-ions and thruster electrons. The presence of CEX-ions and

thruster electrons emerged as a critical factor in determining the spacecraft's final potential when the thruster is active.

The findings for distances ranging from 0.067 AU to 1 AU can be summarized as follows: Firstly, when the SPT-100 hall thruster is operational, the spacecraft maintains a low, stable, and negative potential from -2V to -6V across a wide range of heliocentric distances. The variation in spacecraft potential is reduced significantly compared to when the thruster is off. Without the thruster, the spacecraft exhibits a large variation in potential, ranging from +9 V to -28 V. The negative potentials when the thruster is on are primarily due to the dominance of the CEX ions and thruster electrons over the ambient plasma and the effects of both photoelectrons and secondary electrons. The negative potentials result primarily from the collection of thruster electrons. Secondly, the potential structures of the spacecraft are intrinsically 3D (in detail, rotationally symmetric 2D) with different ram, wake, and side (perpendicular to the ram–wake axis) potential structures due to the importance of the thruster CEX ions and electrons, photoelectric and secondary electron emission (and collection), and the wake void region. These effects often lead to potential hills/wells (depending on particle charge) and associated reflection and trapping effects on particles. In general, these effects appear to combine nonlinearly, and all are quantitatively important, albeit less so when the thruster particles dominate the ambient plasma. Thirdly, during thruster operation, the magnitudes of the changes in the sheath potential and the potential barrier are significantly reduced due to the high dominance of CEX-ions over the ambient plasma. This leads to a less restrictive escape of secondary electrons and photoelectrons, thereby minimizing their recollection. Consequently, low recollection of secondary electrons may reduce the disturbances and enhance the accuracy of low-energy plasma measurements. In contrast, without the thruster, close to the Sun the plasma near the spacecraft experiences a strong potential barrier, which limits the escape of photoelectrons and secondary electrons, resulting in large recollection. In such cases, the spacecraft charges to a large negative potential, and recollection of the low-energy electrons has a high chance of interfering with spacecraft instruments.

Moreover, in close proximity to the Sun, both photoelectrons and secondary electrons play a significant role in reducing the negative potential of the spacecraft (making the potential more positive), regardless of whether the thruster is on or off. Indeed, the absence of photoemission or secondary electrons makes the spacecraft more negatively charged when the thruster is on, albeit to a significantly lesser degree than without the thruster in the absence of photoemission or secondary electrons. Far away from the Sun, near 1 AU, the influence of photoelectrons and secondary electrons is negligible when the thruster is on. However, when the thruster is off, the absence of photoelectrons can lead to high negative charging. In this situation, the operation of the thruster helps maintain and stabilize the spacecraft's potential to a low negative potential. For example, at 1 AU, the spacecraft's potential without the thruster and without photoemission reaches a substantial negative value of -11.1 V. In contrast, with the thruster but without photoemission, the potential stabilizes at -6.7 V. Without the thruster far away from the Sun, secondary electrons have negligible impact on spacecraft potential due to the low mean energy of thermal electrons.

Furthermore, when the thruster is on, the elimination of either photoemission or secondary electrons can lead to higher negative charging of the spacecraft, albeit to a lesser extent when

compared to the combined elimination of both photoelectrons and secondary electrons. On combined elimination, the spacecraft can acquire a considerably high negative potential when the thruster is on, corresponding to these processes combining nonlinearly rather than linearly. For instance, at 0.067 AU from the Sun, when secondary electrons and photoemission are both eliminated simultaneously, the spacecraft becomes charged to a significantly substantial negative potential of approximately -11.1 volts, as opposed to -1.70 volts (when photoelectrons and secondaries are considered).

Lastly, the solar photon flux has a relatively small effect on the spacecraft's potential when the thruster is turned on compared to when it is off, resulting in a significant shift in spacecraft potential. Photoelectric effects always make the spacecraft potential more positive in our simulations, as does secondary electron emission. The accumulation of thruster electrons on the spacecraft's surface depends on the presence and absence of photoemission and secondary emission and the magnitude and sign of the spacecraft's potential.

Overall, these findings have significant implications for how the thruster's operation can assist in maintaining and controlling spacecraft charging under various solar wind conditions. This newfound understanding should aid in enhancing the pre-flight design assessment of electric thruster-induced charging and ensure the safety of sensitive instruments on board. Future studies will evaluate the effects of different electric thruster plumes on the spacecraft potential in the solar wind, magnetospheric environments, and terrestrial LEO orbits.

Acknowledgement

We express our gratitude to the Australian Research Council for supporting the ARC Training Centre for CubeSats, UAVs, and Their Applications (CUAVA), as well as to the University of Sydney and ARC CUAVA for funding the PhD scholarship of the First Author. Special thanks are extended to our industrial partner, Saber Astronautics, for their unwavering support throughout the research. The authors also acknowledge and appreciate the assistance of Fredrik Johansson from the ESA-SPINE Community for providing technical support on the SPIS Software.

Software Availability Statement

The spacecraft charging effects were simulated using the SPIS software (version 6.1.0). SPIS can be downloaded from the official website: https://www.spis.org/software/spis/get/. The spacecraft model is created using the Gmsh software (version 4.10.5) available at: https://gmsh.info/. The original files of spacecarft geometry and meshing file (.geo and .msh), the simulation file (.spis), and the raw data utilised for the analysis in this article are taken from the simulation output folders which are made available at https://hdl.handle.net/2123/31951 [doi: 10.25910/vv3g-zr19].

References

Bigioni, L., & Passaro, A. (2003). Plasma Thruster Plume Simulation: Effect of the Plasma Quasi Neutrality Hypothesis. 34th AIAA Plasmadynamics and Lasers Conference, AIAA-2003-4173, June 23-26, 2003, Orlando, Florida. https://doi.org/10.2514/6.2003-4173

Ergun, R. E., Malaspina, D. M., Bale, S. D., McFadden, J. P., Larson, D. E., Mozer, F. S., et al., (2010). Spacecraft charging and ion wake formation in the near-sun environment. *Physics of Plasmas*, 17(7), 072903-1–072903-9. https://doi.org/10.1063/1.3457484

Filleul, F., Sutherland, O., Cipriani, F., & Charles, C. (2021). BepiColombo: A Platform for Improving Modeling of Electric Propulsion-Spacecraft Interactions. *Frontiers in Space Technologies*, *2*, 639819. https://doi.org/10.3389/frspt.2021.639819

Garner, C. E., & Rayman, M. (2013). In-Flight Operation of the Dawn Ion Propulsion System Through Year One of Cruise to Ceres. *49th AIAA/ASME/SAE/ASEE Joint Propulsion Conference*, 4112. https://doi.org/10.2514/6.2013-4112

Gmsh," Version 4.10.5, [Software]. Available at: https://gmsh.info/.

Goebel, D. M., & Katz, I. (2008). *Fundamentals of Electric Propulsion: Ion and Hall Thruster. Germany: Wiley*.

Guillemant, S. (2014). *Study and simulations of spacecraft/plasma interaction phenomena and their effects on low energy plasma measurements.* PhD Dissertation, Université Paul Sabatier-Toulouse III. https://theses.hal.science/tel-00976017

Reissner, J. L., Tajmar, A., & Jeong, Y. (2011). Simulation of the spacecraft electric propulsion interaction on DubaiSat-2 using SPIS. 32nd International Electric Propulsion Conference, Wiesbaden, Germany, pp. 1-15.

Kuninaka, H., & Kawaguchi, J. I. (2011). Lessons learned from round trip of Hayabusa asteroid explorer in deep space. *2011 Aerospace Conference*, 1-8. IEEE. https://doi.org/10.1109/AERO.2011.5747599

Liu, T. M., & Walker, M. L. R. (2013). Integration of Electric Propulsion Systems with Spacecraft–An Overview. The 33rd International Electric Propulsion Conference, IEPC.

Feng, Na., F., Qizheng, J., Jihao, H., Xu, T., & Yafei, Y. (2019). Numerical simulation of ion thruster plume to spacecraft charging. 2019 14th IEEE International Conference on Electronic Measurement & Instruments (ICEMI), 1555-1561. IEEE. https://doi.org/10.1109/ICEMI46757.2019.9101855

Shinde, T. L., Held, J. M., & Cairns, I. H. (2022). Simulation Study of Hall Thruster and their Effects on the Spacecraft at 1 AU and 0.093 AU. 37 International Electric Propulsion Conference, IEPC-2022-324, June 19-23, 2022.

Shinde, T., Cairns, I., & Held, J. (2023). Charge-Exchange Plasma Effects of the SPT-100 Hall Thruster at Heliocentric Distances from 0.044 AU to 1 AU. *AIAA SCITECH 2023 Forum*, 1597. https://doi.org/10.2514/6.2023-1597

Spacecraft Plasma Interaction Software (SPIS) - Simulation Package for Space Plasma," Version 6.1.0, [Software]. Available: https://www.spis.org/software/spis/get/

Tajmar, M. (2002). Electric propulsion plasma simulations and influence on spacecraft charging. *Journal of Spacecraft and Rockets*, 39(6), 886-893. https://doi.org/10.2514/2.3895

Thiebault, B., Jeanty-Ruard, B., Souquet, P., Forest, J., Mateo-Velez, J. C., Sarrailh, P., et al., (2015). SPIS 5.1: An innovative approach for spacecraft plasma modelling. *IEEE Transactions on Plasma Science, 43* (9), 2546-2557. http://doi.org/10.1109/TPS.2015.2425300.

Torkar, K., Riedler, H. W., Escoubet, C. P., Fehringer, M., Schmidt, R., Grard, R. J. L., et al., (2001). Active spacecraft potential control for Cluster–implementation and first results. *Annales Geophysicae*, 19(10/12), 1289-1302. https://doi.org/10.5194/angeo-19-1289-2001

Torkar, K., Arends, W., Baumjohann, C. P., Escoubet, A. Fazakerley, M. Fehringer, G. Fremuth, H. Jeszenszky1, G. Laky, B. T. Narheim, W. Riedler1, F. R¨udenauer, W. Steiger, K. Svenes, & H. Zhao. (2005). Spacecraft potential control for Double Star. *Annales Geophysicae*, 23(8), 2813-2823. https://doi.org/10.5194/angeo-23-2813-2005

Wartelski, M., W., Matías, Ardura, C., Theroude, C., Reissner, A., Tajmar, M., & Gengembre, E. (2011). The Assessment of Interactions between Spacecraft and Electric Propulsion Systems Project. 32nd International Electric Propulsion Conference, IEPC-2011-028, September 11–15, 2011.

Wartelski, M., Theroude, C., Ardura, C., & Gengembre, E. (2013). Self-consistent Simulations of Interactions between Spacecraft and Plumes of Electric Thrusters. 32nd International Electric Propulsion Conference, IEPC-2013-73, June 6-10, 2013.

Wang, J. (1997). Ion Thruster Plume Plasma Interactions in the Solar Wind.